Chapter 2
How User's Requirements Influence the Development of Scintillators

Abstract In this chapter we discuss practical scintillation parameters which are relevant from a user's point of view for the pragmatic choice of an existing or the development of a new scintillator. For the majority of applications the most relevant ones are density, operation speed, light yield, identification of particles, production capability, stability under ionizing radiation, durability of operational parameters. We describe five main domains of applications, each of them with its own list of requirements: high energy physics, medical imaging, security applications, physics of the universe, and well and mud logging.

For a long time the choice of scintillators has been limited to only a few which were used in a large range of applications. NaI(Tl) is the best example of a material, which, because of its exceptionally high light yield, has been considered as an acceptable compromise for the majority of applications in spite of its low density. However, an important progress in the understanding of fundamental mechanisms underlying scintillation properties as well as in the production technology, a large number of materials available now and a possibility to tune some important properties give a larger flexibility and allow tailoring to some extent the performance of a scintillator to the specific requirements of different end users. Inorganic scintillation crystals are among the most popular ionizing radiation detectors. We consider here the most important inorganic scintillator parameters, which are relevant from a user's point of view for the choice of an existing or for the development of a new scintillator.

1. **High density**. Scintillation inorganic materials, especially synthetic crystalline compounds can reach a density $\rho > 8$ g/cm^3 and even more for lead tungstate crystal (8.28 g/cm^3) and for lutetium aluminum perovskite (8.34 g/cm^3). Moreover, high density reduces the material size of showers for high-energy γ-quanta and electrons, as well as the range of Compton scattered photons for lower-energy γ-rays. This allows a high segmentation of the detector and leads to a better spatial resolution. Finally, high-density materials have generally heavy ions in the lattice, which significantly increases the photo-fraction (~ Z^4). This point is particularly important for some applications like positron emission tomography [1]. This is also important to have a high stopping power for the

P. Lecoq et al., *Inorganic Scintillators for Detector Systems*,
Particle Acceleration and Detection, DOI 10.1007/978-3-319-45522-8_2

electromagnetic component of the ionizing radiation in order to have a compact detector [2].

2. **High operating speed**. Crystalline scintillation materials cover a wide spectrum of scintillation decay times from a hundreds of ps as, for example BaF_2, up to ms or more like Yb^{3+} and Tb^{3+} doped materials. The fastest ones can be used for high counting rates of γ-quanta and in systems where good time resolution is required. The precision of time measurement with a scintillation detector is proportional to $\sqrt{\tau_{sc}}$. The short scintillation decay time is therefore especially important for the measurement of short time intervals and for the operation in fast coincidence circuits.
   The combination of high density and fast response of the scintillation detector gives a unique opportunity to detect rare events in particle physics, particularly, at high luminosity accelerators.
   The very severe requirements imposed by high-energy physics detectors have been since a long time a driving force in the development of new heavy and fast scintillators.
3. **Light yield**. Inorganic crystalline scintillators can have a very high light yield Y as compared to other scintillation materials. Moreover, the room temperature specific light yield $S_{\tau_\tau} = Y/\tau_{SC}$ (number of photons emitted in unit time) of some of them is even greater than the one of liquid xenon. As the precision of timing measurements with scintillation detector is proportional to $1/\sqrt{S_\tau}$ and the energy resolution measured in the given time interval is proportional to $\sqrt{Y}$, a high light-yield scintillator allows one to achieve the best combination of energy and time resolution in a wide γ-quanta energy range. The search for a scintillation material with a combination of high stopping power, high time response and good photo-absorption peak resolution was strongly motivated by the development of new express methods in well-logging.
4. **Particles identification**. A good feature of inorganic scintillators is that the scintillation detector response is proportional to the particle energy deposited in the material in a large energy range. However, the slope is different for charged particles, ions, and γ-quanta [3]. Therefore inorganic crystalline scintillators might be applied to identify particles and γ-quanta in fluxes of mixed interaction products.
5. **Volume**. The worldwide capacity of modern crystalline scintillator growing facilities allows the production volume of up to several cubic meters in a relatively short time. This makes it possible to build huge detectors and to study rare events resulting from the interaction of the accelerated particles or from space origin. In comparison with Cerenkov and liquefied gas detectors, inorganic scintillators have incomparably greater values of specific light yield per unit volume of the material, which makes them rather attractive for space experiments applications. On the other hand, the same property allows, for example, building very compact detectors for medical devices like intravenous and per operative probes.

6. **Parameters stability under ionizing radiation**. Scintillation inorganic crystalline materials have in general a good stability of their parameters even in the presence of intense ionizing radiation environment. This property is crucially important for the measuring systems used in space, well logging and high-energy physics experiments at high luminosity accelerators. The high stability of scintillation properties of inorganic materials under ionizing radiation is related to a high level of production technology, which guarantees the production of single crystals with a very low level of uncontrollable structural defects.
7. **Durability of operational parameters**. Similarly to other crystalline materials having a high structural quality, scintillation crystals maintain their physical-chemical parameters for a long time. Although not addressed frequently, this point is of key importance for experiments having a long lifetime. This is caused by a high degree of internal symmetry in the material, which results in their high energetic stability. For this reason, several planed experiments in high energy physics which have a duration from the design phase up to the data analysis of 10–15 years are using crystalline inorganic scintillators for their electromagnetic calorimeter.

However, it is generally impossible in practice to find a scintillator, which combines all these attractive properties. The choice of a material currently existing or to be developed will be therefore tailored to the user's requirements as a function of the priority given between the above-mentioned parameters. A large fraction of the scintillator market is driven by X-rays and γ-rays spectroscopy for a wide range of applications. The authors expect the reader to be introduced to general spectroscopy methods and techniques, which are anyway well described in many books. We consider here six main domains of applications, each of them with its own list of requirements:

- High-energy physics and particle detectors;
- Spectrometry of low energy γ- quanta;
- Application in medical imaging;
- Safety Systems;
- Space application;
- Well and mud logging.

High Energy Physics is a driving force in the development of new scintillation materials, due to the very challenging requirements of modern experiments as well as to the large volumes of scintillators needed. As a recent example the design and construction of new experiments to be installed at the Large Hadron Collider (LHC) at CERN has required a new detector component able to maintain a high stability of optical parameters under long-term exposure to ionizing radiation. In fact, at the beginning of the 1990s, the LHC program initiated a variety of research and development projects to make possible the design and construction of detectors with unprecedented performance. The lead tungstate $PbWO_4$ scintillator is the result of one of these successful projects. It is a good example of scintillator material engineering by a multidisciplinary community of material and technology

scientists and high-energy physicists. Within 5 years the crystal production technology has evolved from the production of a few samples to the mass production of about one thousand of crystals with specified parameters per month. PWO crystal was used to build the Electromagnetic CALorimeter (ECAL) and the Photon Detector of the CMS and ALICE experiments at CERN, respectively. It has been selected to build the ECAL of the PANDA experiment at the FAIR (GSI, Darmstadt). It is also the most attractive candidate to build or upgrade several small set-ups for the intermediate energy region, where fast response and good energy resolution are required. A similar situation was previously observed with the development of CsI crystals for the BELLE collaboration.

2.1 User's Requirements for High Energy Physics

2.1.1 Introduction

The discovery of α particles by Rutherford in 1899 was made possible because of the invention by Crookes a few years before of a device, called spinthariscope, which made use of the scintillating properties of Lead Sulfide. Indeed, scintillators were already involved in what can be considered as the first High Energy Physics experiment, and that was the beginning of a long common story.

When Hofstadter [4] introduced in 1948 Thallium doped Sodium Iodide, NaI (Tl), he probably did not realize that it was going to be the most popular scintillator for the next 35 years. The best example of the high discovery potential of scintillators in High Energy Physics was first given by the NaI(Tl) Crystal Ball experiment at SLAC [5] which allowed reconstructing the precise spectroscopy of charmonium particles (Fig. 2.1).

But in the last two decades a new generation of HEP experiments has become a driving force for the development of new scintillators. This has started with Bismuth Germanate (BGO) for L3 [2] and Cesium Iodide (CsI either Thallium doped or pure) for CleoII [6], Crystal Barrel [7], KTeV [8], Belle [9] and BaBar [10], which were already known but in small sizes and small quantities only. It became even more evident with Barium fluoride (BaF_2) for TAPS [11] and GEM [12], Cerium Fluoride (CeF_3) as a candidate for CMS [13] and L3P [14] and finally Lead Tungstate ($PbWO_4$) for CMS [13] and Alice [15] at the CERN Large Hadron Collider (LHC), which were essentially developed for HEP experiments. This chapter will describe how the difficult physics constraints and harsh experimental conditions impose very tight specifications to modern detectors. The size of the experiments and the high quantitative demand allowed organizing the R&D effort on a large scale. This has been particularly illustrated by the work of the Crystal Clear Collaboration [16], which was able to create a multidisciplinary effort to make the best use of cross-fertilization between different categories of experts and industry to develop suitable scintillators at an industrial scale.

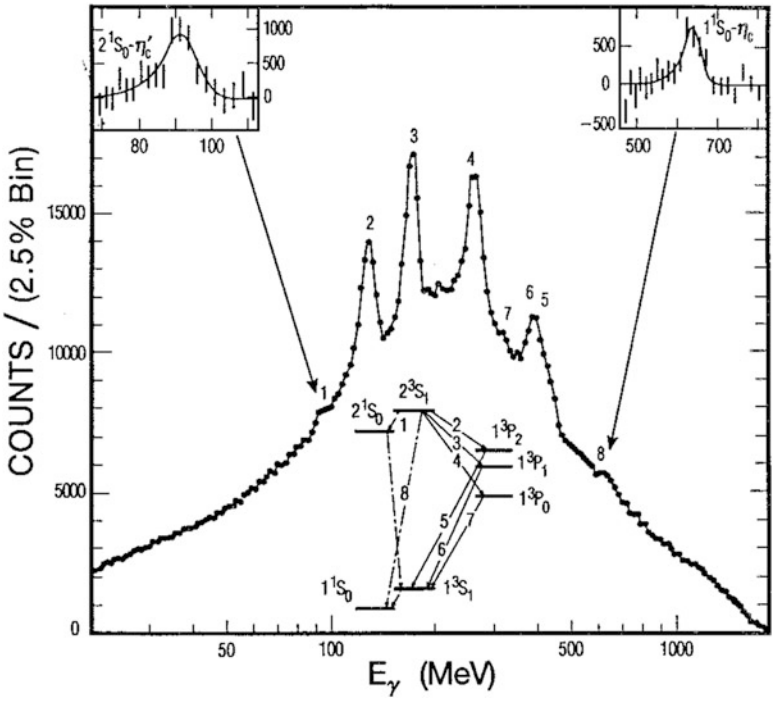

Fig. 2.1 Charmonium spectroscopy with the Crystal Ball at SLAC [5]

A better understanding of some basic mechanisms of energy relaxation, scintillation process, and radiation damage is progressively being built through this common effort. The immediate consequence is to allow a much faster and much more efficient development of scintillators for other detectors in High Energy Physics, but also for other applications and particularly for industrial and medical imaging devices.

2.1.2 Physics Requirements for High Energy Physics Experiments

One of the main motivations for the construction of the CERN new proton-proton collider LHC was the study of the symmetry breaking mechanism, which is supposed to be responsible for the generation of the masses of the particles in the electroweak theory. One or several scalar bosons (the Higgs bosons) are involved in this mechanism and can be detected through their leptonic and $\gamma\gamma$ – decay modes. The main argument, generally used to stress the high level of performance required for the detectors, is the detection of 2γ resulting from the decay of the Standard Model Higgs boson, for which the natural width is completely dominated by the

instrumental resolution below Higgs masses of ≈ 200 GeV/c^2. As this signal is associated with a very high background, generated by a combination of π° also decaying in 2γ, and the direct production of photons via the quark-quark, gluon-gluon and higher order diagrams, the signal to noise ratio is dominated by the photon detector energy resolution.

Usually electron and photon energies are measured in detectors called calorimeters, where they are stopped, producing a shower of secondary particles. In sampling calorimeters the photon energy is converted in high-density absorber plates, and a small fraction of the energy is measured in a sensitive medium interleaved with the absorption medium. In a homogeneous detector, on the other hand, the electron or photon showers are fully contained in the sensitive medium. The energy is then revealed by scintillation or Cherenkov light, both collected in highly transparent media or by ionization in conductive liquids, where charges are collected.

The mass resolution of a particle, which is detected through the two-photon decay channel, depends on the energy resolution and angular divergence θ [radian] of two quanta with energies $E_{\gamma 1}$, $E_{\gamma\ 2}$ [GeV] as

$$\frac{\delta_M}{M} = \frac{1}{2}\left[\frac{\delta E_{\gamma_1}}{E_{\gamma_1}} \oplus \frac{\delta_{E_{\gamma_2}}}{E_{\gamma_2}} \oplus \frac{\delta_\theta}{\tan(\theta/2)}\right] \tag{2.1}$$

Homogeneous detectors are well known to give an excellent energy resolution, which is usually parameterized in the following way:

$$\delta E\gamma/E\gamma = a/\sqrt{E} \oplus b \oplus c/E, \tag{2.2}$$

where a is the statistical term (sampling or fluctuations of all sorts), b is the constant term, c is the energy noise equivalent term.

High precision calorimetry at the future proton-proton machines requires an energy resolution of the order of 0.5 % for 100 GeV photons.

A homogeneous calorimeter is not limited by sampling fluctuations and an energy dependant term of the resolution "a" as small as 2 % has been currently achieved on several large size calorimeters. It is much more difficult to achieve a constant term "b" of ≈ 0.5 %. On large systems like the L3 BGO calorimeter at CERN, one recognizes usually 3 contributions to the constant term:

$$b^2 = b_{\mathrm{L}}^2 \oplus b_{\mathrm{F}}^2 \oplus b_{\mathrm{c}}^2$$

The $b_{\ \mathrm{L}}$ term represents the fluctuations due to the energy leakage. The front leakage due to backscattered particles has a negligible contribution above a few GeV. Having sufficient material for full longitudinal energy containment can easily control the rear leakage. For the photon energies up to 100 GeV, at least 25 radiation lengths are necessary to maintain the leakage term within reasonable limits (one radiation length is the mean distance over which a high-energy electron loses all but

1/e of its energy). The side leakage is more difficult to control. It is determined by the number of cells one has to sum-up to reconstruct the energy with sufficient precision. On the other hand, this number is limited by the electronic noise and chiefly by the multiple event pile-up at LHC if the shower spreads too much laterally. Low noise electronics and high-density material will of course limit this contribution. A particular attention must be paid to all gaps, walls, and dead material in front, which may have an important contribution to the leakage term. All leakage contributions can be well reproduced by Monte-Carlo and a b_{L} term of $\approx$0.3 % can be achieved with a crystal calorimeter.

The b_{F} term is associated to non-uniformity. They can result from non-homogenous active material, like variation of doping concentration in non-intrinsic scintillators. Temperature gradient can be the dominant factor of non-uniformity when there is a strong dependence of the light yield with the temperature (Lead Tungstate for instance has a large temperature coefficient of $-1.9\,\%/\,^{\circ}\mathrm{C}$). Crystals like Cerium Fluoride (CeF_3), with a temperature coefficient as small as $1\,\%/\,^{\circ}\mathrm{C}$ near room temperature will be insensitive to this effect. Other sources of non-uniformity are associated to the light collection. Pointing geometry implies cells of pyramidal shape. The light focusing effect in these cells, particularly if the refraction index of the medium is high induces a strong non-uniformity. CeF3, with an index of 1.6 is here again much better than BGO (n = 2.15) or PWO (n = 2.28). Finally much attention should be paid to avoid large absorption of the light in the medium. This is perhaps the most important problem for crystals with an emission spectrum in the UV like BaF_2 and other cross-luminescent crystals, as well as for low-density materials because of the long path-length of the photons to reach the photo-detector. For dense crystals with an emission spectrum in the visible, a bF term as small as 0.25 % can be obtained.

The last contribution b_{C} corresponds to the inter-calibration errors. Frequent calibrations with an efficient monitoring system are necessary to maintain this contribution below 0.3 %. The L3 BGO has proven that a well-designed fiber monitoring system can maintain the inter-calibration within 0.3 % for long periods of time and more than 10000 crystals. The high luminosity pp machines will also provide excellent means for a continuous calibration of the detector. At LHC a rate of 10 Hz is expected for electron pairs from Z° decays in the central region, which should allow a weekly calibration with about 100 electrons per channel. If there is a good inner tracker, individual e^+ or e^- can be used (E/p matching) at a rate, which could be as high as 100 per channel and per day. Finally one should be able to take advantage of the copious number of minimum ionizing particles for an almost continuous inter-calibration control of all the channels. The CMS PWO calorimeter is aiming at a precision of 0.2 % for the determination of inter-calibration constants.

Taking all these contributions together it seems that a constant term b = 0.5 %, although difficult, is not out of reach for a well-designed homogeneous calorimeter. Figure 2.2 shows the energy resolution in the required energy range for several already existing or proposed detectors.

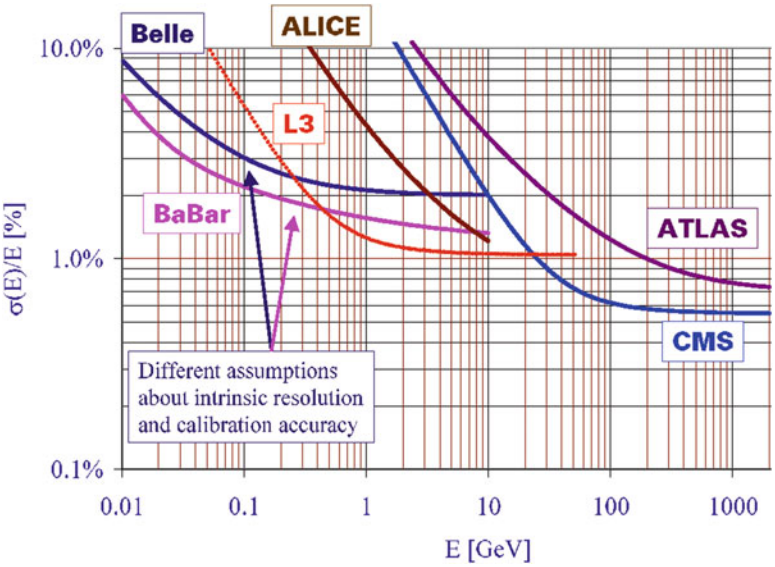

Fig. 2.2 Energy resolution of several HEP calorimeters (Courtesy of P. Denes, LBL)

2.1.3 Scintillator Requirements for High Energy Physics Experiments

The criteria for the choice of the scintillator are based on the density, the scintillation properties and the radiation hardness. The cost is also an important issue taking into consideration the very large volumes of several cubic meters considered for such detectors.

2.1.3.1 Density

The compactness of the calorimeter is essential in order to reduce the detector volume and cost. This is achieved by using high stopping power materials resulting in a small radiation length X_0. A high-density material ($\rho > 5$ g/cm^3) is therefore needed, but not necessarily with very high Z components as it is often quoted. The density should be preferably based on a high compactness of the crystal lattice (a large number of atoms per unit volume), keeping the atomic number of the components not too large in order to reduce the lateral shower size (Moliere radius: $RM \approx X_0\ (Z + 1.2)/37.74$). A small Moliere radius will limit the contamination of the energy measurement by other particles from the same or other events (pile-up) and help for the position reconstruction as well as for the π^0 rejection, which will be

the dominant background at LHC. Finally a compact material will reduce the lateral spread of the shower in a high magnetic field.

2.1.3.2 Scintillation Properties

The pile-up will impose severe constraints to the readout, particularly at LHC. It is therefore essential to collect as much signal as possible within one bunch crossing (25 ns), to keep a good signal to noise ratio in the electronics chain, and to reduce the fluctuations due to the timing jitter. Decay times of the order of the bunch crossing time or even less are necessary. Only optically allowed (inter-configuration) transitions (like the transition $5d \rightarrow 4f$ for Ce^{3+}), cross-luminescence, which is intrinsically fast and temperature independent, and strongly quenched intrinsic and activator's luminescence can give rise to a fast and bright scintillations.

As the electromagnetic calorimeter is usually installed in a magnetic field, readout by photodiodes or avalanche photodiodes is desired. These photo-detectors have a gain with is either 1 for PIN diodes or of q few hundreds in the case of avalanche photodiodes, which is significantly lower than photomultipliers. This implies a sufficient light yield (a few 100 pe-/MeV of deposited energy), and an emission wavelength above 250–300 nm, where the quantum efficiency of the photodiodes becomes high. A light emission in the visible spectrum will also ease the problems of light collection in long crystals.

The energy resolution of the calorimeter will strongly depend on all possible sources of non-uniformity. The light collection in a pointing geometry will introduce non-uniformity due to the focusing effect, which depends on the refractive index of the crystal. Fluoride crystals and glasses, with refractive index around 1.5 will limit this effect to a much smaller value (and therefore make it much easier to correct) than for the BGO (index 2.15) or PWO (index 2.3). The material can be intrinsically luminescent if it holds luminescent ions, or doped with a scintillating impurity. Intrinsic scintillators are generally preferred, as it is easier to control the light yield uniformity in long crystals. On the other hand, a controlled distribution of the doping could help correcting for the non-uniformity caused by the light collection in a pointing geometry. In addition the scintillation yield should be as independent as possible from the temperature. Large temperature coefficients increase the complexity of the detector and of the software corrections, and temperature gradients between the front and back face of the crystals introduce non-uniformity's affecting the constant term of the resolution.

2.1.3.3 Radiation Hardness

It is now well established that the most significant damage in the majority of inorganic scintillators results from the formation of color centers in the bulk of

the material, which absorb part of the scintillation light on its path to the photodetector [17]. More details are given in Chaps. 6 and 7. A short radiation length will therefore reduce the total attenuation for a given damage. In addition, as most of the color centers absorb mostly in the UV (more precisely they involve traps which are in the vicinity of the fundamental absorption edge), crystals emitting light in the visible are likely to be less severely damaged. Some surface effect may also occur but it is generally very small and saturates quickly with the dose.

The formation of color centers results from the trapping of electric charges by crystal structural defects or impurities and is therefore directly correlated with the quality of the raw material. A large effort should be made to purify the raw materials to the best quality. However, in some cases, a specific doping of the crystal has proved to be an efficient and economical way of significantly increasing the radiation hardness [18].

2.1.4 Cost Considerations

The factors building-up the price of crystals must be identified and carefully analyzed. In some cases, the raw material of the desired purity can represent a substantial fraction of the cost. For this reason, all crystals based on the very rare Lutetium are discarded for applications were tons of crystals are needed, although some of them are very fast cross-luminescent materials ($BaLu_2F_8$) or very efficient scintillators (LSO:Ce). Cerium is much more favorable, as it is the most common of the rare-earth components. The purification of Cerium against the other rare-earth components may be difficult and expensive, but our first studies show that this is not a critical parameter. The growing technique and the crucible material are dominant parameters and crystals, which can be grown for instance by using the relatively cheap Bridgeman method in graphite crucibles, have obvious advantages. The cost of the energy plays also an important role, as a combination of the melting temperature and the pulling rate. From this point of view, the high melting point of GSO or LSO (>1900 °C) and the high cleavage susceptibility of this matrix implying a low pulling rate (1–2 mm/h) may put some limits to the minimum obtainable price for such a crystal. On the other hand, the low melting point of PbF_2 (822 °C) and $PbWO_4$ (1123 °C) and the abundance of the raw material make them low cost materials similar to NaI(Tl). A high crystal density, directly limiting the total volume for a calorimeter, but also the crystal dimensions and consequently the furnace and crucible sizes will be a major parameter of the total cost for a crystal based detector. Finally, the very good mechanical properties of $PbWO_4$ or for instance, allow a high production yield of the mechanical processing, also reduced the final cost.

Table 2.1 Scintillators used in HEP calorimeters (Courtesy of P.Denes)

	NaI(Tl)	BaF_2	CsI(Tl)	CeF_3	BGO $Bi_4Ge_3O_{12}$	PWO $PbWO_4$
Xo [cm]	2.59	2.03	1.86	1.66	1.12	0.92
ρ [g/cm^3]	3.67	4.89	4.53	6.16	7.13	8.2
τ [ns]	230	0.6 620	1050	30	340	15
λ [nm]	415	230 310	550	310 340	480	420
n@λ_{max}	1.85	1.56	1.80	1.68	2.15	2.3
LY [%NaI]	100	5 16	85	5	10	0.5

2.1.5 *Crystal Calorimeters in the World*

The continuous increase of the energy obtained in particle accelerators puts more and more emphasis on calorimetry as a tool to analyze the products of the collisions. As at the same time the proportion of interesting events is becoming smaller and smaller, the demand for high precision homogeneous calorimeters is continuously increasing. This is why the last 20 years have seen a dramatic boost in the development of scintillators and associated readout techniques, directly related to a dozen of projects of impressive dimensions. The properties of the crystals used in these calorimeters are listed in Table 2.1 where some qualitative figures of merit are also indicated, in particular the relative volume needed per unit of stopping power (radiation length x Moliere radius).

2.2 Spectrometry of Low Energy γ-Quanta. Non-linearity of Scintillator Response

The majority of scintillation materials combining at least two from a list of properties which make an "ideal scintillator" including high light yield, high density, fast response and low price, can be used to detect low energy ionizing radiation. This wide branch of detector applications includes devices for research,

spectroscopy, medical diagnostics, geological and geophysical investigation, ecological monitoring, as well as devices of monitoring for technological processes and security systems.

The linearity of the scintillation detector response with energy and a high resolution are crucial features for precision spectrometry. The proportionality between scintillator light yield and energy of ionizing radiation is based on the fundamental principle of electronic excitation multiplication in the scintillation crystal [19]. The first studies of scintillator properties [20, 21] have shown that their response is dependent on the type of ionizing radiation. Only for electrons they have shown a good linearity with energy up to 10 MeV. The linearity of the response of different scintillators to γ-quanta and electrons has been confirmed in many measurements performed in the region up to 100 GeV [3]. However more detailed studies have shown a variation of the proportionality between light yield and energy for soft γ-quanta in the energy range below 1 MeV and especially near the K, L edges absorption of the heavy ions of the scintillator host matrix [22, 23]. The nature of this phenomenon will be described in detail in Chap. 5.

The classical approximation of scintillator efficiency given in Chap. 1 does not imply an evident dependence of the scintillation yield on the absorbed electron or photon energy. However this phenomenon is well known since the discovery of scintillation materials. The most commonly used scintillator NaI(Tl) was described in 1948 [4] and 1 year later [24] it was observed that the light output of this material is not proportional to the energy released in the crystal for photon energies less than 1 MeV. This phenomenon is still under extensive investigation in many scintillators [22, 24–31].

The non-linearity of the light yield with the energy of the detected γ-quanta or electrons has a strong impact on the energy resolution. This intrinsic light yield non-proportionality (sometimes referred to as nonlinearity) is particularly effective at low energies. The best energy resolution in a scintillator can only be achieved when there is a combination of high absolute light yield, good matching of the scintillator emission spectrum with the photo-receiver sensitivity and good proportionality to the energy of γ-quanta or electrons deposited in a crystal. The non-proportionality manifests itself as discontinuities of the light yield around the K- or L-edge of heavy atoms in most inorganic scintillators [30].

It is presently impossible to predict the response linearity of a given material although it is certainly related to some non radiative relaxation or quenching effects in the case of high ionization density. So far only $YAlO_3$: Ce (YAP) and to some extent ZnSe:Te [32] have a good energy resolution down to a few keV.

There have been several studies to simulate the electron energy distribution produced in a scintillator by the interactions from incident photons. Based on Monte Carlo simulation results electron energies were determined by considering Compton scattering, photoelectric absorption and pair production interactions separately [29]. These simulations have shown good agreement with experiment at least for several materials such as NaI(Tl), CaF_2(Eu) and LSO. The comparison of these simulations with experimental data for electrons and photons interacting with

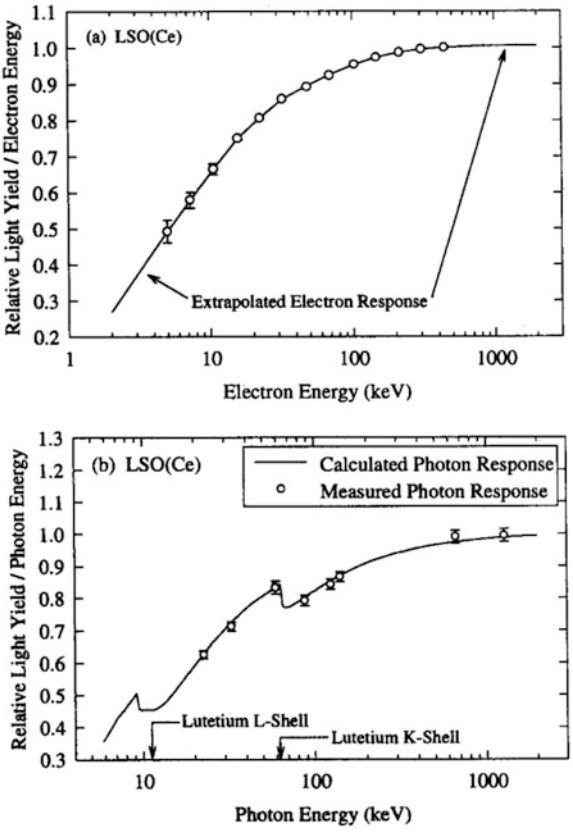

Fig. 2.3 (**a**) – LSO:Ce electron response with low and high energy extrapolations, (**b**) – calculated photon response along with measured data for same crystal that was used to measure electron response in [30]

LSO:Ce is shown in Fig. 2.3. The good match of the simulation and experimental data allows considering optimistically the theoretical prediction of non-proportionality in new materials.

This effect has no practical implication for high energy physics detectors but it is on the other hand of prime importance for high precision spectrometry in the medium energy range. The LSO:Ce crystal, which is a very successful material for medical imaging applications, has its advantage of a high light yield severely balanced by a poor linearity for energies below 1 MeV.

It has to be noted, that till now a detailed theory of spectroscopic properties of scintillators does not exists. The existence of different approaches to the description of the non-proportionality at low energy range is an example of the complex nature of this phenomenon. The most linear scintillator is YAP:Ce, so we shall consider its spectroscopic properties in details.

This scintillation material has been discovered in the seventieth, however large scale applications have started a few years later with the development of the production technology of crystals with high light yield [33–42].The comparison

Table 2.2 The basic performances of crystal YAP:Ce in comparison with NaI (Tl)

Material	ρ, g/cm^3	$Z_{eff.}$	Y, %	Refraction index n	$\lambda_{em.}$, nm	τ_{sc}, ns	Y temp. coeff at room temp., %/°C	Hardness (Moos)
NaI(Tl)	3.67	50	100	1.85	410	230	0.2–0.95	2
$YAlO_3$:Ce	5.55	36	40	1.94	347	28 ± 2	0.39	8.5

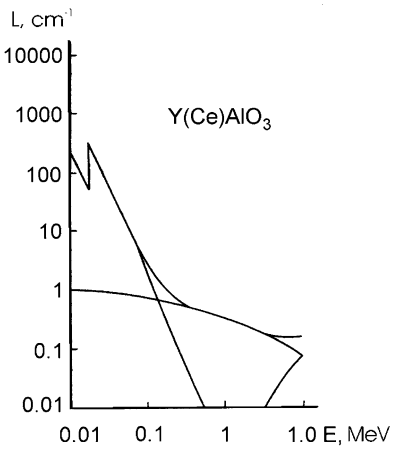

Fig. 2.4 Dependence of the linear attenuation factor L on energy of γ-quanta in $YAlO_3$:Ce single crystal

of scintillation and some physicochemical performances of $YAlO_3$:Ce and NaI (Tl) are shown in Table 2.2. The dependence of the linear attenuation factor *L* with energy and amplitude spectra of some soft γ-quanta is shown in Figs. 2.4 and 2.5. The unique detecting properties of YAP:Ce scintillator makes possible its wide use in Mössbauer spectroscopy which is one of the most powerful structural-analytical research techniques of condensed matter.

The efficiency of the transmittance Mössbauer spectroscopy is proportional to the count rate of the detector [43]. The fast scintillation time of YAP:Ce gives therefore a significant advantage on NaI(Tl) or even on cooled semi-conductors in spite of a worse energy resolution. YAP:Ce-based detector crystal of 0.35 mm thickness has allowed increasing by one order of magnitude the efficiency of measurements with a ^{57}Co (Rh) source of 2 GBq activity.

A distinctive feature of $YAlO_3$:Ce scintillator is the weak dependence of the light yield with temperature (Fig. 2.6). It makes possible its use in extreme temperature conditions, for example, in systems of continuous check of steel band, well logging, space etc.

Besides spectrometry in the 1–100 keV range, YAP:Ce crystals have very good energy resolution near half of a MeV. An energy resolution of 4.38 % FWHM has been measured at 661.6 keV (^{137}Cs), [44], better than the 6.6–6.8 % energy resolution gained with reference scintillation NaI (Tl) crystal. This apparent paradox for

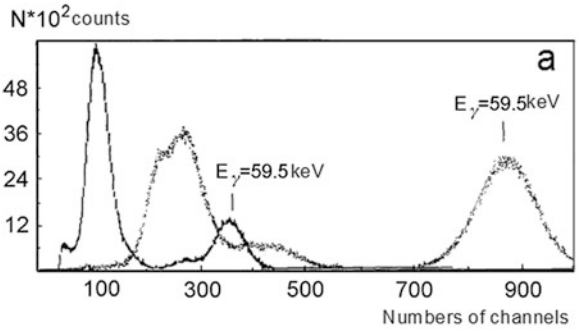

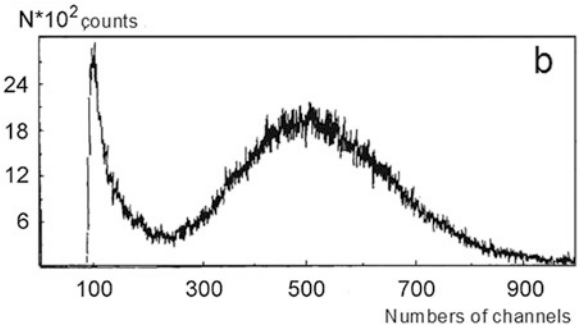

Fig. 2.5 ^{241}Am isotope amplitude spectrum (**a**), NaI (Tl) ∅ 25 × 1 mm (*dots*); $YAlO_3$:Ce ∅ 25 × 0.35 mm (*continuous line*), (**b**) – spectrum of ^{55}Fe measured with the same YAP:Ce, T = 300 K

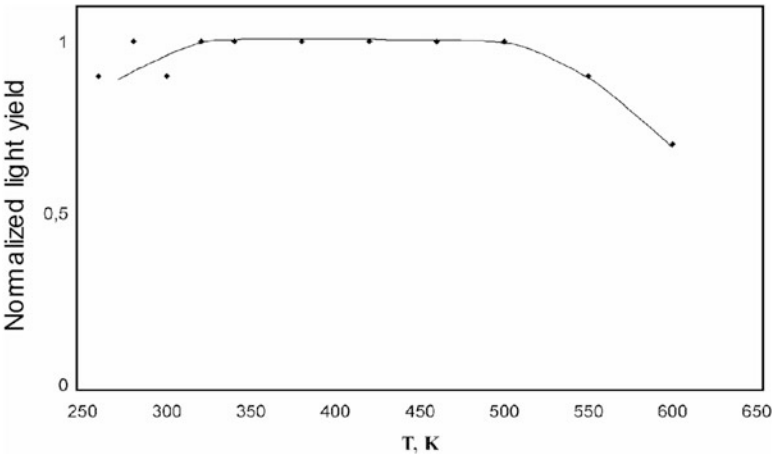

Fig. 2.6 $YAlO_3$:Ce scintillator light yield dependence versus temperature

a crystal having a light yield of only 40 % of NaI(Tl) is a direct consequence of a much better low energy linearity of YAP:Ce than NaI(Tl). A similar situation is illustrated by the LuAP:Ce crystal, which has at least the same energy resolution as LSO:Ce in spite of a light yield a factor 2 to 3 smaller.

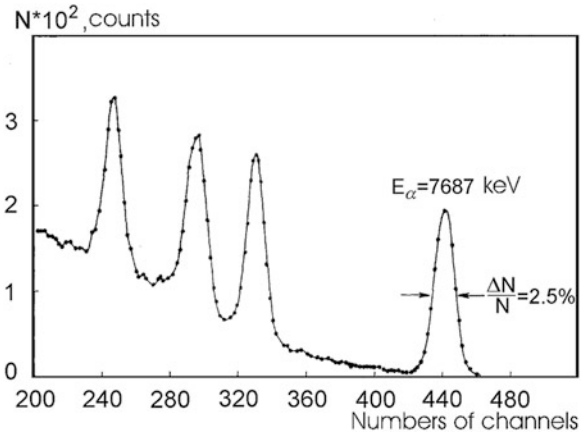

Fig. 2.7 An energy distribution of α-particles emitted by ^{226}Ra source

Another important application of $YAlO_3$:Ce crystals is the detection of α-particles. The mean free path of α-particles in YAP is 8–28 μm in the energy range 4–8 MeV. The light yield ratio γ/α is 3.8. The minimization of the γ-quanta contribution to the noise is achieved by the use of thin crystals. YAP:Ce crystals with a thickness of less than 100 μm are easily produced now. Figure 2.7 shows the ^{226}Ra source amplitude spectrum measured with a ∅ 25 × 0.1 mm YAP:Ce crystal collimated by a 1.5 mm diameter hole in a 2 mm thick aluminum foil. This is a good setup for low background spectrometry of α-particle emitting isotopes.

The spectrometric performance of other scintillators is also widely described in the literature [45]. Alkali halide scintillators are still the most used for routine measurements in the range up to 10 MeV, mostly because of their well-developed production technology and low cost. However this situation is changed in favor of oxide materials when the combination, of at least a high light yield, fast response and high stopping power is required. We can easily predict that scintillators based on complex structure oxides will dominate in the next 5–10 years.

2.3 User's Requirements for Medical Imaging

2.3.1 Introduction and Historical Background

At the same time Rutherford was studying α particles on a Zinc Sulfide scintillating screen, Wilhelm C. Roentgen, also using a similar device, was able to record the first X-ray picture of his wife's hand. That was probably the first example of technology transfer between particle physics and medical imaging, and the beginning of a long common history.

The interest for Thallium doped Sodium Iodide, NaI(Tl), introduced in 1948 by Hofstadter [4] was suddenly boosted by the invention in 1958 of the Anger camera

concept [46], where a large NaI(Tl) slab is readout by several photomultipliers (PMT), allowing a relatively precise determination of the γ conversion point. This invention offered unprecedented perspectives in the field of nuclear medicine imaging and non-invasive clinical investigations. Several imaging devices have been built with a large number of NaI(Tl) crystals arranged on a sphere (hair drier) or on a circle (hair shrinker) around the head of a patient. But in spite of its very high light output Sodium Iodide suffers from a relatively low density (3.67 g/cm^3), which limits the spatial resolution and the image quality.

It is worth noting that several important contributions to medical imaging were made by physicists: Allan MacLeod Cormack (tomography principles); Felix Bloch, Edward M. Purcell, Peter Mansfield, (resonance imaging), Georges Charpak (digital radiography). It relates not only to the basic principles, but to the many details of radiation detection technologies. The anatomic and functional image fusion – the last trend in medical diagnostics was also proposed by David Townsend, a CERN physicist. This situation can be easily explained keeping in mind the similarity of multidetector systems in HEP and medical imaging systems. In some cases scintillators primary studied as an option for one HEP project found later an application in radiation medical diagnostics.

Bismuth Germanate (BGO) discovery is one of the typical examples of such "transfer". This scintillator invented in 1973 by Weber & Monchamp in 1973 was immediately recognized for its potential for γ-cameras, because of its very high density (7.12 g/cm^3). But systematic use of BGO in medical imaging could only be made possible through the large effort of the L3 collaboration at the CERN LEP collider, to develop with several companies low cost mass production technology for BGO, in particular with the help of the SIC in China. Today BGO still represents a very large fraction of the γ-ray medical imaging market. The example of LSO is just opposite: first developed for well logging it is now the most popular crystal for PET scanners and it is seriously considered for several HEP detectors.

The need for high density but much faster scintillators for the new generation of hadron colliders triggered a large R&D effort worldwide in which the Crystal Clear collaboration at CERN [16] has played a major role since 1989. New crystals have been developed, like Lead Tungstate (PWO), which will be the basic element of the largest crystal calorimeter ever, build for the CMS experiment at LHC, with nearly 100 tons of crystals. Moreover systematic study of the physics underlying the fundamental scintillation mechanisms has led to a much better prediction capability in the search for new scintillating materials. New ultra dense, very fast and efficient scintillators are being studied and are now in the phase of the mass production technology development. Several of them have a high potential for medical imaging devices.

2.3.2 The Different Medical Imaging Modalities

The field of medical imaging is in rapid evolution and is based on five different modalities: X-rays radiology, emission tomography, ultrasonic tomography,

magnetic resonance (MRI) and electrophysiology with electro- and magneto-encephalography (EEG and MEG). More recently direct optical techniques like bioluminescence and infrared transmission are also emerging as powerful imaging tools for non-too deep organs. Only X-rays radiology and emission tomography are using scintillators and are described here in more details. Total volume of scintillators for medical application exceed few hundred tons [47].

2.3.2.1 X-Rays Radiology

This is the most popular technique, which comprises X-ray Radiography, Computed Tomography (CT), and Tomo-Densitometry (DXA). The general trend is to progressively replace the film by digital devices, as already used for CT. Besides direct conversion detectors like amorphous Silicon or CdZnTe, scintillation materials are widely developed for this application. For small scintillation screen thickness (0.1–0.2 mm), which is well adapted to the lowest X-ray energies (for instance about 20 keV for X-ray mammography), ceramics are well adapted. On the other hand for dental X-ray diagnostics (about 60 keV) and full body X-ray computed tomography (about 150 keV) the required stopping power would need much thicker screens. This would induce too much light yield loss when classical ceramics screens are used. A large R&D effort is under way by several companies to replace them by detector arrays made of CsI(Tl) needles or small crystals (for example calcium tungstate CaWO or YAP) directly coupled to photodiode arrays or segmented photomultipliers.

2.3.2.2 Scintillators for CT Applications

Single Crystalline Materials One of the most widespread scintillator applications in medical diagnostics is CT imaging (X-ray Computed Tomography). The principle of CT is based on the detection of X-ray attenuation profiles from different irradiation directions. This technique allows a 3D reconstruction of attenuation density within the human body. These density profiles can then be viewed from different directions and analyzed in a succession of slices allowing a full 3D reconstruction of the anatomical image.

The X-ray detector is typically built up by using a scintillation material coupled to a photosensitive array of Si-diodes. There are several specific sensor properties requirements (such as high X-ray absorption, spectral correspondence of scintillator emission and photo-receiver efficiency, hard radiation stability and low afterglow level [48]) that define the limits for the search of new CT scintillation materials [48, 49].

Among them, the material stability under X-radiation, light output temperature stability and a minimum level of afterglow are certainly the most critical in comparison with any other applications [48, 50]. Modern X-ray CT system is

producing about 1000 projections (subject slices) per second. This imposes severe constrains on both the decay time and afterglow. Afterglow is known to produce ghost images through a "memory effect" which deteriorates the quality of the images. The main parameters of scintillators used for CT systems are listed in Table 2.3.

Historically, the first material for this application was CsI(Tl) with a high light output green emission matching well the maximum sensitivity of Si photodiodes. However, the scanning speed increase resulted in high, rigid demand to suppress the afterglow, and even the best CsI(Tl) samples could not satisfy the requirements for the new scanner generation. This is why CsI(Tl) has been progressively replaced by $CdWO_4$ (CWO), which is now the basic component of all modern CT devices.

For CWO detectors the conversion factor is about 0.01 electrons/eV [50]. A high detector conversion factor and good crystal uniformity are mandatory for a high contrast resolution over a wide range of X-ray attenuation. But the main motivation to use a new material was the possibility to reduce the afterglow at a level of 0.005 % in 3 milliseconds after the irradiation. So far this result remains unsurpassed.

Another important parameter for such applications is the light yield stability under temperature changes or irradiation.

Temperature Dependence of Detector Gain The temperature dependence of the luminescence yield $I(T)$ under excitation at 300°K is explained in terms of the probability of non-radiative transitions by the Mott's equation $I(T) \approx (1 + \omega_0 \exp(-\varepsilon/\mathrm{k}T))^{-1}$ [51] with frequency factor $\omega_0 = 4.25 \cdot 10^6$ and thermal activation energy $\varepsilon = 0.49$ eV. As was shown in [50], this theoretical curve coincides well with the temperature dependence of the CWO crystal and the CT detector response. This value is not the best among CT scintillators, but satisfies current engineering demands.

Radiation Damage In medical CT the maintenance of the system imposes a continuous exposure to radiation and the crystals accumulate a certain level of radiation damage. This could result in variation of sensitivity and deterioration of the accuracy of the system. The typical exposure rate of a CT scanner is about 1Rad/s. However due to a strong absorption in the scintillator entrance face, the dose rate could exceed ~50 Rad/s in this part of the crystal that may lead both to detector gain drift and spectral sensitivity loss, and finally to the crystal deterioration. The main part of the scintillation efficiency degradation is recoverable after 1 h of relaxation. It means that the CWO exploitation has to take into account the balance between the accumulation and recovery of radiation damage. There are several channels of radiation induced scintillation losses like decrease of crystal transparency [53] and variations of luminescence yield due to modifications of the emitting centers [49]. Radiation damage effects are related to internal crystal defects, deviation from stoichiometry and traces of impurities. These phenomena and potential CT scintillator improvements will be discussed in Chaps. 6 and 7.

Table 2.3 Scintillators characteristics for CT [51–53]

	CsI-Tl	BGO	CWO	$(Y,Gd)_2O_3$:Eu	Gd_2O_2S:Pr, Ce,F
Type	Single crystal	Single crystal	Single crystal	Ceramic	Ceramic
Density, g/cm^3	4.52	7.13	7.99	5.9	7.34
Thickness to absorb 99 % (90 %) of 145 kV X-ray, mm*	6.1(2.2)	2.8(1.2)	2.6(1.1)	5.8(2.2)	2.9(1.1)
Emission band max, nm	550	480	495(580, 690)	610	520
Light output, % NaI-Tl	85	9	38	34	51
Conversion factor, eV/el	45	450	100	–	–
Decay time, s	1	0.3	2, 15	1000	~2.4
Afterglow, %(ms)	0.5–5(6)	0.005(3)	0.005(3)	0.1(100)	0.01(3)
Temp. stability, %/°C, at 25 °C	0.02	−0.15	−0.30	<0.04	−0.6
Rad. damage, % per (R)	+13.5(450)	–	−1.8(775)	−1.0(450)	–

Ceramics Materials In spite of their wide use CWO crystals are not the ideal choice for CT application due to their brittleness and the toxicity of Cadmium. This has been an argument for the search of a new generation of CT scintillators. This search was initiated by General Electric and Siemens in the mid of 80th when they introduced the first polycrystalline ceramic scintillators. The host materials were Y_2O_3 and Gd_2O_3 and their mixtures [54], after doping by Pr and Tb, demonstrated reasonable properties. Nevertheless their transmission was rather low, ceramics being more translucent than transparent. The Eu^{3+} activator efficiently traps electrons to form a transient Eu^{2+} state, allowing holes to form Pr^{4+} and Tb^{4+} and, therefore, competes with the intrinsic traps responsible for afterglow. This energy trapped on the Pr and Tb sites decays non-radiatively in presence of the Eu ions reducing therefore the level of afterglow [54].

3 mol% of Eu_2O_3 doping to $(Y,Gd)_2O_3$ allows to reach 65 % of CsI(Tl) efficiency with emission at 610 nm. The relatively long decay time (~1 msec) can be accepted because of the low afterglow level.

Gd_2O_2S:Pr,Ce,F ceramics has a shorter decay time, a higher light output, a low afterglow, but the emission peak is at 511 nm, which is less convenient for Si photodiodes.

These two types of ceramics known as UFC and Hilight are widely used in off-the-shelf CT scanners. However, the search for more efficient ceramics continues. $Gd_3Ga_5O_{12}$:Ce,Cr [48] is considered to be a good candidate. During the last years Lu_2O_3:Eu, Tb were investigated also. But at this stage the afterglow level is relatively high and will be a major limitation if no solution is found to suppress it.

$SrHfO_3:Ce^{3+}$ and $BaHfO_3:Ce^{3+}$ ceramics are other candidates for both CT and probably PET devices [48]. Both of them are high-density materials, have a short decay time and reasonable light yield (up to 20000 photon/MeV). Moreover their afterglow level is small.

Recently, a new generation of high light yield scintillation ceramics with garnet structure produced by High Temperature High Pressure (HTHP) method was introduced [55, 56]. HTHP method is melt free and allows producing complex compositions of the materials combining more than three oxides. This technology opens an opportunity for future progress in engineering of scintillation properties.

These examples show that new materials investigation and research remain highly topical and that the potentialities resulting from the impressive progress in nanotechnologies to produce new transparent ceramics will offer new perspectives for CT scanners.

Detector Engineering The demand for a better spatial resolution for X-ray CT scanners and the progress in photo-detectors PSPMT (Positive Sensitive Photo Multipliers) and Si-photodiodes matrixes have triggered a strong development effort for pixel based arrays and matrixes design. The main applications for such devices are X-ray CT and industrial and security systems.

Linear scintillation arrays are widely used in CT systems with two main designs: ladder type scintillators and medical CT linear arrays.

The first type of arrays coupled to Si-photodiodes is based on pixels of 1–2 mm in cross section and up to 2 mm in thickness. The typical number of pixels varies from 8 to 16, 32 or even 64 in such arrays. They are mainly based on $CdWO_4$ and CsI(Tl), although some ceramic scintillators are also available now.

The second type requires thicker pixels. Typical sizes are: $(1–2) \times (20–30) \times (2–3)$ mm^3. It reflects the necessity of multi slice image reconstruction for medical analysis.

Two-dimensional arrays for medical applications were designed over 30 years ago. The first prototypes were based on NaI(Tl) crystal that required hygroscopic protection and had a big gap between elements due to MgO powder used as light collector and for optical separation of pixels. Important progress of 2D matrix design was correlated with the development of advanced photodiode matrixes in the last 10 years. Such "sandwiches" have a better spatial resolution and real time visualization potential.

Last years' engineering efforts showed that multilayered assemblies [57] initially developed for astrophysics detectors can be efficiently used for medical applications.

State-of-the-art array design is based on minimization of the two main parameters: pixel size and gap between pixels. These issues are critical to reach the best spatial resolution and to minimize losses inside the gap between pixels.

Pixel Size The choice of the scintillating material is of course the key for a higher segmentation of a new generation of CT scanners. The choice of the material is also important because the pixel size is determined by mechanical properties of the crystal like hardness, cleavage, machining ability etc. Thus, the minimal pixel size is now slightly different for various materials, namely, 0.3 mm for CsI(Tl), CWO, and BGO; 0.5 mm for CaF_2:Eu and LSO.

It should be noted, that so small pixel size will lead to a considerable increase in the number of channels to an increased complexity of the acquisition system. However, CCD matrixes having tens millions of pixels per cm^2 are available to date. Thus, there are no technical limits to read so called columnar structure screens [58, 59].

The example of flat panel development shows that matrix detectors and flat screens could be developed from two different production technologies of the same scintillator. Other materials could follow the same route. A typical example is the ceramic material Gd_2O_3S:Tb for X-ray intensifying screens [60, 61]. The emission at 545 nm is very convenient for coupling to photodiodes with a sensitivity peak in the green-red range of the spectrum. Recently, Agfa introduced a 43×43 cm^2 flat panel based on this material deposited on a matrix a-Si:H photodiodes (pixel size 160×160 μm^2). This is practically the same size as was achieved for CsI (Tl) screens.

BaFBr:Eu [62] is the typical inorganic stimulated phosphor for digital radiography. A more detailed review of these materials is available in [47, 48, 60].

It should be noted that it is possible to use non-pixilated screens for the low energy X-rays. If X-rays are absorbed in a very thin crystal layer, the angle of the

emitted light is small (for the thin film) and the crosstalk to the neighbor photo receiver is negligible maintaining therefore a good spatial resolution. The search for materials for such applications is of very high importance now.

Separator Size and Thickness Separators are put into the gap between crystal pixels to prevent the photon leakage from pixel to pixel. It is obvious that this material should be as thin as possible, possess good reflectivity and low transparency. Practically used materials are: white powder (TiO_2, MgO, more than 1 mm thick, reflectivity 100 %), Teflon, Tyvek™ sheets (0.5–0.15 mm thick and 98 % reflectivity) and aluminized composites (VM2000 type, about 0.1 mm thick and 95 % reflectivity).

Each pixel geometry and matrix design depends in general on the array specification. Modern specifications require less than 2–4 % cross talk (leakage) between neighbor channels. Powder reflectors, as well as thin films (like Teflon, Tetratex, BHA films), possess the best reflectivity, but they are not suitable for the bonding process. They need also to be relatively thick to have good properties. White paints and/or epoxy covering is suitable for relatively large-sized pixel designs. Metals (lead, tungsten or tantalum) prevent optical leakage between matrix elements, but do not allow reaching a good reflectivity. At the same time, the metal separator can absorb the radiation incident to the separator surface before it strikes the light sensor. These metallized films (like VM2000) are the most appropriate materials due the best balance of reasonable reflectivity, thickness and cross talk.

Total light collection in a matrix element (linear array) depends on separator type and reflectivity as well as crystal surface conditions. These conditions are important not only for the best light output, but also for the best uniformity and minimal spread of the data from pixel to pixel. The non-uniformity of the best matrixes should not exceed 2–5 %. Such rigid specifications require good and very uniform crystal surface treatment. The large quantity of elements in 2D matrix does not allow checking each element. Good surface quality should be obtained from a minimum number of mechanical operations. Crystal damage, sub-surface intrinsic stresses and material recrystallization at the production stage may deteriorate the performance of some pixels. The light output spread for the same CsI(Tl) elements might reach 15 %. When the surfaces are treated in a slightly different way.

The matrix uniformity is based on high accuracy and low cross dimensions tolerances. For hard materials (BGO, CWO, GSO) these tolerances should not exceed +/− 0.01–0.02 mm and could even reach the level of about 50 microns. For the soft scintillators (like CsI) this value is always higher.

2.3.2.3 Emission Tomography

The working principle of emission tomography is to image γ-rays emitted by radiotracers injected to the patient. Contrary to X-ray CT and nuclear magnetic resonance, which provide very precise images of the anatomy of organs, nuclear imaging modalities give in vivo access to the functioning of these organs.

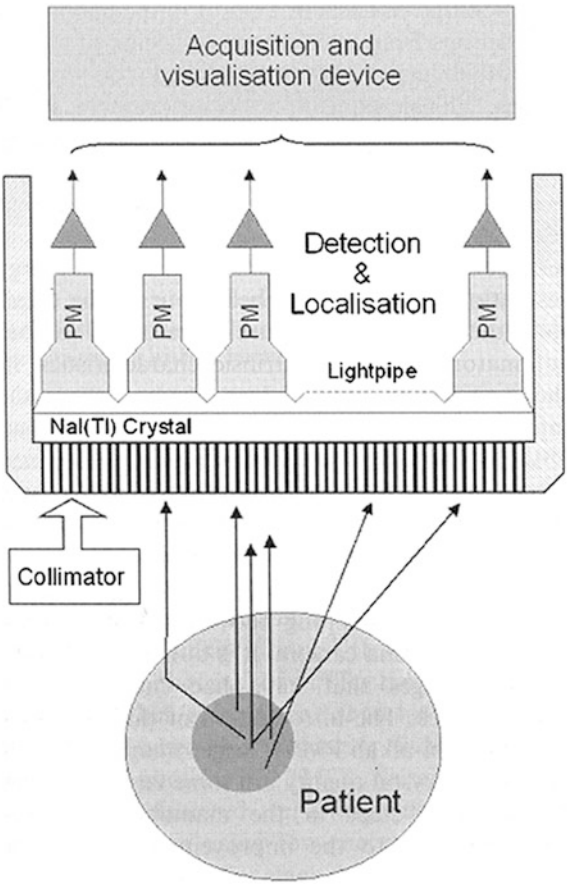

Fig. 2.8 Principle of the Anger camera

SPECT Tomography In Single Photon Emission Computed Tomography (SPECT) a molecule involved in the metabolism of the patient is labeled by a single photon emitter (usually ^{99}Tc emitting one 140 keV γ-ray). After injection it concentrates in some organs or tumors and allows the imaging of them by the reconstruction of the γ-ray emitting points. The most popular technique is based on the "Anger logic" [46], where γ-rays are directed through a multi-hole collimator to a large slab of NaI or CsI scintillator (Fig. 2.8).

The coordinates of the interaction point are then determined by comparing the signals from a set of PMT's coupled to the crystal, by the centre of gravity method. This technique is still largely used in many hospitals and medical imaging labs, but suffers from a relatively poor space resolution, of the order of a few centimeters. A modern approach uses the direct coordinate determination with Position Sensitive PMT's (PSPMT) coupled to scintillation multi-crystal array based on CsI or YAP crystals. Several devices have been developed, like HIRESPECT, a YAP mammography camera in Italy with a resolution of 0.7 mm, as well as peroperative probes.

The Anger logic proved to be quite effective (the same principle was earlier applied for astrophysical telescope design [63]) with a good price-performance ratio. Indeed a detector for whole body screening (i.e. with a cross section up to 600×500 mm) may be completed with 35–40 PMT. (The practice shows, that the replacement of 3″ PMT by 2″ PMT, the use of hexagonal and square PMTs does not significantly improve the resolution of the whole system). The above engineering solution has therefore remained almost unchanged up to now and SPECT diagnostics is still the most largely used method of nuclear medicine. There is today no real alternative to NaI(Tl) crystals. Only scintillators with a significantly better energy resolution (approx. 3–4 %) could make a step forward. Recently $LaCl_3$:Ce or $LaBr_3$:Ce [64, 65] have been discovered, however their application is still limited by the cost of these materials and the difficulty to produce them in large size.

A more realistic alternative is CsI(Na) halide scintillators in large monoblocks and CsI(Tl) pixilated (matrix) detectors, which are used, in portable cameras. Continuous CsI(Na) crystals $50 \times 50 \times 4.6$ mm with white entrance and black edge reflecting was used for a flat-panel-based mini gamma camera for lymph nodes studies [66]. The intrinsic resolution level of this system is better than 1.5 mm. This system is therefore competitive with more complex pixilated designs [67]. Some investigations [67, 68] confirmed the ability to reach almost the same system efficiency when using pixilated, partly pixilated and continuous detectors and demonstrated the flexibility of the detector design to optimize its performance.

A CsI(Tl) crystal coupled to a photodiode allows to significantly reducing the size of the detector while maintaining a good sensitivity. Such a design includes 4096 scintillation pixels. The DIGIRAD imager (pixilated detector size of 21×21 cm) has been evaluated during a clinical myocardial study [69]. This detector is smaller in size than a conventional gamma camera detector, and can be used as portable gamma cameras complementing the whole body systems.

Such functional system designs may compete with direct converters based on semiconductors (CdTe, CdZnTe etc.). These systems have a better energy resolution, but their use is presently limited by a low production yield and the technical problems to produce high-grade semi conducting crystals with good uniformity.

It must be noted that some attempts a few years ago to use two SPECT cameras in coincidence in order to obtain a pseudo PET system (of rather limited performance) has led to the development of 25 mm thick NaI(Tl) plates able to record with a reasonable sensitivity 511 keV γ-quanta [70–74].

Positron Emission Tomography Positron emission tomography (PET) makes also use of molecules involved in different metabolic functions of the human body, allowing therefore precise functional imaging. They are labeled here with β^+ emitter isotopes, which are generally produced in a cyclotron. These PET tracers, injected into a patient, simulate natural sugars, proteins, water and oxygen presence in human body. The Positron Emission Tomography measures the uptake of the tracer in different organs or tumors and generates an image of cellular biological activities. These PET images can be used to quantitatively measure many

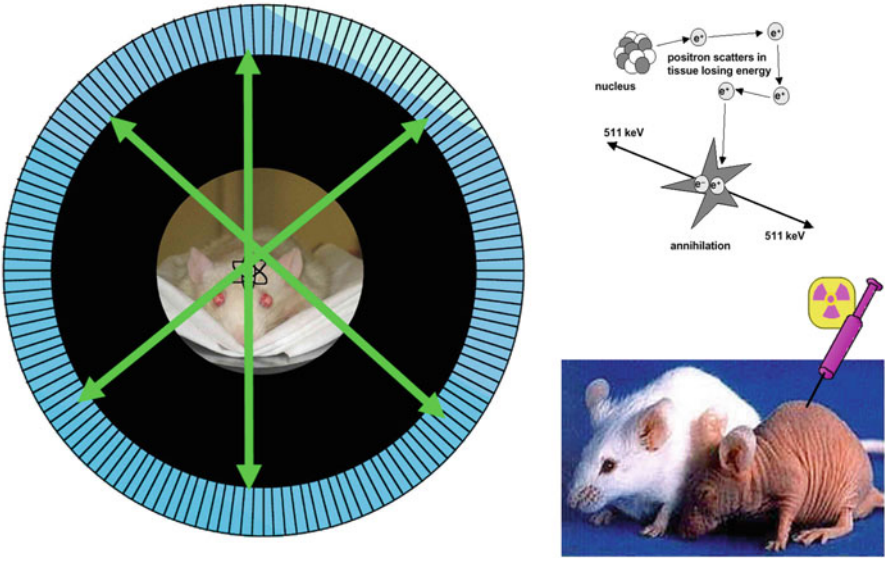

Fig. 2.9 Working principle of a PET scanner

processes, including sugar metabolism, blood flow and perfusion, oxygen consumption etc. Recently, the need for specialized PET scanners designed for experimental small animal studies (mouse, rat, and rabbit) was recognized as a powerful tool for fundamental research of disease models, new therapeutic approaches and pharmacological developments. The most commonly used isotopes are ^{18}F with a lifetime of 109.8 min, ^{11}C (20.4 min), ^{13}N (10 min) and ^{15}O (2.1 min), which are all among the basic building blocks of organic systems and can therefore easily be chemically introduced in molecules involved in metabolic or pharmaceutical reactions. A typical example is FDG (fluorodeoxyglucose), which allows monitoring the energetic consumption of the cells in different parts of the body. Once fixed in some organs or tumors, the molecule emits positrons decaying in 2 back to back γ-rays, which are detected in coincidence in rings of scintillators (Fig. 2.9). Until recently, as a result of compromise between performance and cost, PET scanners were using partially segmented BGO crystals readout by groups of 4 PMT's, allowing a reconstruction precision of the order of 4 to 5 mm (Fig. 2.10). Modern machines are going progressively to higher segmentation of the crystals and of the readout to achieve higher spatial resolution. Resolutions of the order of 1 mm are considered to be within reach. Another important parameter is the sensitivity, which relates the number of useful detected events to reconstruct an image to the dose injected to the patient.

It must be noticed that PET scanners allow localizing radiotracers uptakes in the human body but do not deliver precise anatomical images, like MRI or X-ray CT for instance. A new generation of scanners combines the very high sensitivity of

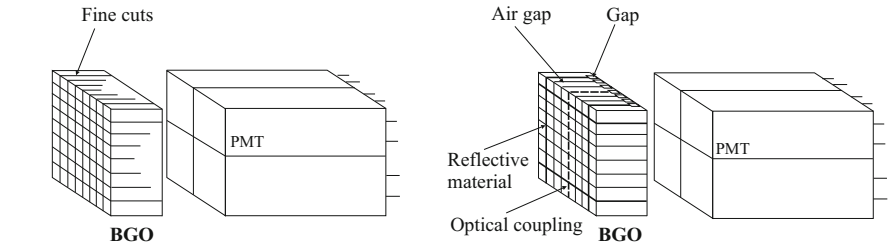

CTI EXACT design
with pseudo-discrete matrix with light share at the bottom of the block

GE Advance design
with discrete matrix with light share along the length of the element

Fig. 2.10 PET detector module design

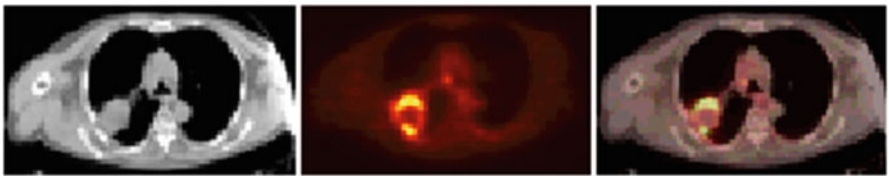

Fig. 2.11 Primary lung cancer imaged with the SMART scanner. A large lung tumor, which appears on CT as a uniformly attenuating hypo dense mass, has a rim of FDG activity and a necrotic center revealed by PET (Photo courtesy of D. Townsend, University of Tennessee)

PET for metabolic imaging to the high spatial resolution anatomic information delivered by X-ray CT or another anatomical modality. They provide impressive images giving the very precise localization of active areas of organs and tumors (Fig. 2.11). PET scanners are very powerful tools for basic research in cognitive sciences, clinical oncology and kinetic pharmaceutical studies.

Requirements for an Optimal Scintillator The first important requirement for a scintillator to be used in medical imaging devices is the stopping power for the given energy range of X and γ-rays to be considered, and more precisely the conversion efficiency. Clearly materials with high Z and high density are favored but the position of the K-edge is also important as can be seen on Fig. 2.12. For low energy X-ray imaging (below 63 keV) the attenuation coefficient of Yttrium, Cesium and Iodine are quite high and crystals like YAP and CsI are good candidates. Above the K-edge of Lu (63 keV) and Bismuth (90 keV) the situation is quite different and BGO and Lutetium based crystals will be clearly favored for 99Tc (90 keV) SPECT and PET scanners (511 keV). Heavy scintillators are also useful to reduce their thickness and the parallax error in ring imagers.

A short absorption length is important not only to increase the number of detected X or γ-rays for a given detector thickness but also to maintain a good spatial resolution over the whole field of view. A short crystal will reduce the effect

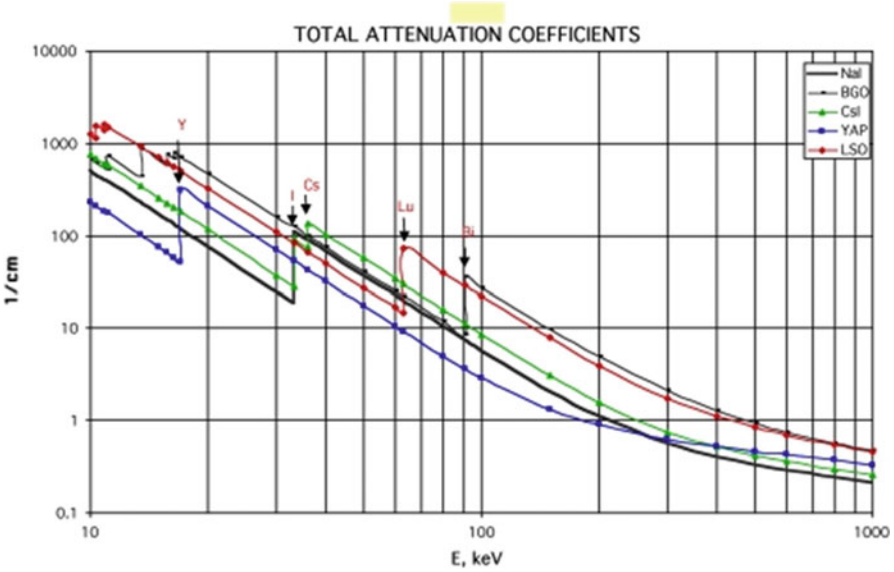

Fig. 2.12 Attenuation coefficient in several high Z materials

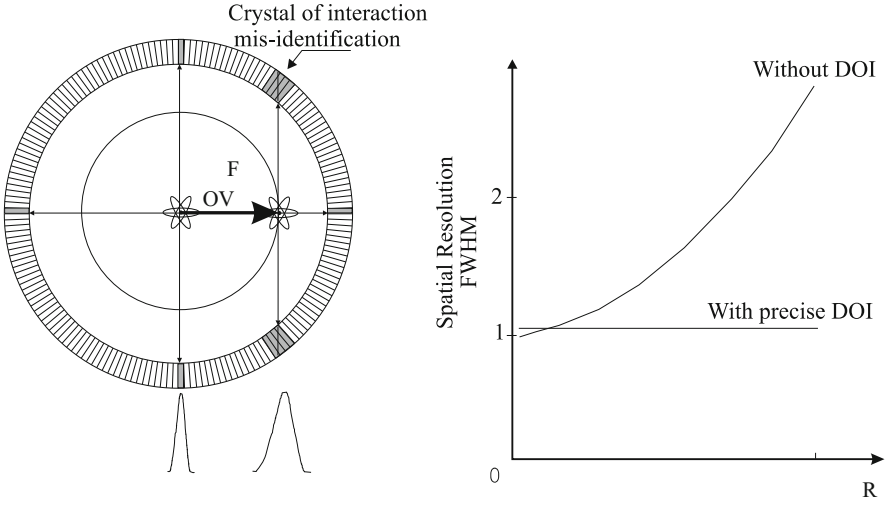

Fig. 2.13 Radial elongation distortion in a PET scanner

of the radial elongation as shown in Fig. 2.13. Another approach is to use a combination of two or more crystals mounted on top of each other (phoswich configuration) with different emission wavelength or decay time so that the depth of interaction (DOI) determination is made possible through the correct identification of the crystal hit.

A high light yield is also mandatory to improve the energy resolution, which is essentially limited by the photo statistics and the electronic noise at these energies. A better energy resolution allows a higher rejection of Compton events and improves therefore the spatial resolution and the sensitivity. The sensitivity is a very critical parameter of nuclear medical imaging as it reflects the number of useful events per unit of injected dose to the patient. A higher sensitivity means a smaller injected dose or a better image contrast.

A short scintillation decay time allows reducing the dead time and therefore to increase the limiting counting rate. Moreover by reducing the coincidence gate the signal to background ration is improved which has a direct impact on the image quality. Here again the sensitivity and image contrast are increased for a given patient dose, or the dose can be reduced. It must be noticed that very fast scintillators can open the way to scanners using the time of flight information, which will help reducing the background by selecting a narrow region of interest along the coincidence line.

Sodium Iodide (NaI) and more recently Cesium Iodide (CsI) have been for a long time the most common scintillators used in nuclear medical imaging devices, mostly because of their very high light yield and relatively easy and cheap production methods. But their low density and slow decay time considerably limits the performance of these devices. The large effort made by the L3 collaboration at CERN to develop cheap mass production technology of BGO crystals has introduced this material in the field of medical imaging, mostly because of its very high density and conversion efficiency. Most of the PET scanners produced in the last decade were built with BGO crystals. Unfortunately a much smaller light yield than NaI and a decay time of 300 ns are still limiting factors.

There is a need for a crystal having the light yield of NaI, the density of BGO, but at least 10 times faster than BGO. What matters in fact is the largest possible number of photons emitted in a short gate of typically a few tens of nanoseconds. This crystal has been developed since about 15 years. This is the Lutetium orthosilicate LSO:Ce and its variation LYSO:Ce with a few percent of Yttrium substituting to Lutetium ions. LSO and LYSO are progressively replacing BGO in modern PET scanners. During the last decade the Crystal Clear collaboration at CERN has been deeply involved in the development of another attractive crystal in this category, the Lutetium Aluminium perovskite LuAP:Ce, also with the Yttrium heavily doped compound LuYAP:Ce [75, 76]. This crystal has a much better linearity at low energy than LSO, which results in an even better energy resolution in spite of a light yield about a factor 2 smaller. Moreover its properties perfectly match the one of LSO, which makes the combination LSO-LuAP the ideal phoswich for depth of interaction determination.

There are a number of other possible candidates for PET applications that are being studied by different groups. They are listed in Table 2.4.

If we restrict this list to crystals having a light yield of more than 10^4 ph/MeV and a decay time of less than $\tau_{sc} \leq 100$ ns the number of good candidates is restricted to ten only: Lu_2S_3, $LuAlO_3$, Lu_2SiO_5, $Lu_2Si_2O_7$, $LuBO_3$, $LaBr_3$:Ce, $CeBr_3$, $PrBr_3$, $GdBr_3$:Ce and $Gd_3Al_2Ga_3O_{12}$:Ce from which five are complex oxide compounds.

Table 2.4 Properties of scintillation materials with high photo-absorption coefficient

Material	ρ g/cm^3	Z_{eff}/photo-abs. Coeff. at 511 keV, cm^{-1}	Y, ph/MeV	τ_{sc}, ns	$\lambda_{s\,c}$, nm	S_τ ph/MeV/ns	$1/\tau_{sc\text{II}}$, MHz
$BaLu_2F_8$	6.94	63/0.22	870	1 + slow	313	870	1000
$BaLu_2F_8$:Ce	6.94	63/0.22	400	35 + slow		11	30
LuF_3:Ce	8.3	61.1/0.31	8000	23 + slow	310	347	43
Gd_2O_2S: Pr,Ce,F	7.34	61.1/0.21	40000	2100	580	19	0.4
Lu_2S_3:Ce	6.2	66.7/0.24	28000	32	592	875	31
$CdWO_4$	7.9	64.2/0.26	19700	2000	495	9.85	0.5
$ZnWO_4$	7.87	62.5/0.27	21500	22000	480	0.97	0.05
$CaWO_4$	6.1	63.8/0.22	6000	600	430	10	1.7
$PbWO_4$ (PWO)	8.28	75.6/0.48	100	6	420	17	170
$Bi_3Ge_4O_{12}$ (BGO)	7.13	75.2/0.37	8200	300	505	27	3.3
$Lu_3Al_5O_{12}$:Sc	6.7	62.9/0.21	22500	610	270	37	1.6
$LuAlO_3$:Ce (LuAP)	8.34	64.9/0.29	11400	17 + slow	365	670	58
Lu_2SiO_5:Ce (LSO)	7.4	66/0.28	27000	40	420	675	25
$Lu_2Si_2O_7$:Ce (LPS)	6.23	64.4/0.21	30000	30	380	1000	33
$CeBr_3$	5,2		58,000	21	360, 380		203
$PrBr_3$:Ce	5.3	46.9/	21000	8, 22	365, 395		204
$LaBr_3$:Ce	5.1	46.9/	73000	30	375		205
GdI_3:Ce	5.2		44000	45, 250	560		206
$Gd_3Al_2Ga_3O_{12}$:Ce	5.1		46000	80, 800	520		207
$LuBO_3$:Ce	7.4	64.5/0.28	26000	39	410	660	26

2.4 Radiation Detection for Security Applications

The security system development is carried out in accordance with the Global Nuclear Detection Architecture (GNDA), where radiation detectors and radiation sensors are a significant part. In the 90s, the main attention was paid to military and defense applications; the issue was finally regulated in the frame of the Nunn-Lugar program for the control of dissemination of nuclear weapons. Later, the protection from terrorism and technological catastrophes (like Fukushima) started dominating. Security has been a problem for airlines since the 1970s, when hijackings and bombings became the method of choice for subversive, militant organizations around the world. Although security at transport has always been tight, the 9/11 attacks woke many people up to a harsh reality. It was and is still not tight enough.

During the last decades the radiation detection safety/security market has significantly changed due to the expanding geography of nuclear power plants, as well as growing homeland security and defense claim.

Increasing nuclear threat or nuclear terrorism is driving the homeland security and defense R&D and detector market. Due to 9/11 and Fukushima disasters the homeland security and defense industry has become the fastest-growing segment of the radiation detection, monitoring, and security market and is expected to reach $232.4 million by 2020 from $152.3 million in 2014 [301]. This is a significant part of the whole manufacturing industry.

There are many standards that describe the requirements to radiation monitoring in general and detector devices in particular. They specify different areas of control like "Performance Criteria for Alarming Personal Radiation Detectors" (ANSI N42.32), "Hand-held Instruments for the Detection and Identification of Radionuclides" (ANSI N42.33 and N42.34), "Evaluation and Performance of Radiation Detection Portal Monitors" (ANSI N42.35), "Performance Criteria for Spectroscopy-Based Portal Monitors" (N42.38), "Standard for Performance Criteria for Neutron Instruments" (N42.39) and other.

Science and technology plays a crucial role in the prevention of nuclear and radiological terrorism. All applications of scintillators are directed to one of the two applications: active or passive detection systems. There are four main areas of safety detector equipments using scintillators: inspection of luggage, track and cargo containers inspection, search for nuclear fissile and explosive materials, and remote detection of fissile materials.

2.4.1 Passive Detection

Passive devices provide Security, Customs and Border Protection with a passive, non-intrusive means to screen objects for the presence of nuclear and radionuclide materials: various types of radiation emanating from nuclear devices, dirty bombs, special nuclear materials, natural sources, and civilian/industrial isotopes. Passive

detection is based on scintillators for the detection of gamma and/or neutron-induced fission.

The first generation of radiation portal monitors (RPM) was based on plastic scintillators and did not operate in a spectrometric mode. RPM consisting of large-area γ-ray detectors (usually plastic) and neutron detectors (He-3 or similar) allowed the passive detection of nuclear or other radioactive materials in cargo containers or trucks entering a port of entry. The high detection sensitivity of RPMs allows 100 % scanning of cargo with minimal impact on throughput. However, false positive alarms resulting from cargo which is naturally radioactive can slow-down the flow of commerce. In 2005, the USA Domestic Nuclear Detection Office (DNDO) began working on a program to develop a next-generation of Advanced Spectroscopic Portals (ASP), which was designed to both detect radiation and identify the source as benign, suspect, or threat. The initial concept of the program was to develop, procure, and deploy enough ASPs to replace many of non-spectroscopy devices and handheld detectors at a cost of $2–3 billion [77].

The main goal is the separation of military, technologically enhanced NORM (Naturally Occurring Radioactive Material), like Uranium series (^{238}U), Thorium series (^{232}Th), and Potassium (^{40}K), and Man-Made Sources (e.g. commercial isotopes ^{241}Am, ^{133}Ba, ^{137}Cs, ^{57}Co, ^{60}Co, ^{192}Ir, ^{226}Ra, ^{252}Cf, nuclear fuel, medical radioisotopes ^{99m}Tc (92 % of procedures)). Finally, ASPs were developed and test procedures verified [78], but not put into the force [79]. In 2015 a similar global program was launched and developed [80] in China.

The smallest (hand-held) devices are addressing the instruments that can be used for security applications to detect and identify radionuclides, for gamma dose rate measurement, and for indication of neutron radiation. The performance testing requirements for portable radiation survey meters are listed below and divided into four different categories:

- Nuclear Materials: ^{233}U, ^{235}U, ^{237}Np, Pu*;
- Medical radionuclides: ^{18}F (PET), ^{67}Ga, ^{99m}Tc, ^{111}In, ^{123}I, ^{125}I, ^{131}I, ^{133}Xe, ^{201}Tl;
- Industrial radionuclides: ^{57}Co, ^{60}Co, ^{133}Ba, ^{137}Cs, ^{192}Ir, ^{241}Am;
- Naturally occurring radioactive materials (NORM): ^{40}K, ^{226}Ra (in equilibrium with daughter's products), ^{232}Th and decay products, ^{238}U and decay products.

*Monitors shall identify either weapons grade plutonium or reactor grade plutonium (>12 % ^{240}Pu).

The radiation detector shall be able to identify the following radionuclides within the times indicated after exposure to the radionuclide.

- Unshielded, in 1 min: ^{111}In, ^{133}Xe, ^{99m}Tc, ^{201}Tl, ^{67}Ga, ^{125}I, ^{123}I, ^{131}I, ^{18}F(PET),
- Behind 3 mm steel shielding, in 2 min: ^{235}U, ^{238}U, ^{57}Co, ^{241}Am, ^{237}Np,
- Behind 5 mm steel shielding, in 2 min: Pu*, ^{233}U, ^{133}Ba, ^{40}K, ^{226}Ra, ^{232}Th, ^{137}Cs, ^{60}Co, ^{192}Ir. > 6 % ^{240}Pu.

The requirements to RPM are stricter due to the volume of the subject to be scanned and time limits for the moving subject inspection (For mobile – ANSI N42.43 "Standard for Mobile and Transportable Systems").

The devices shall be able to identify the following radionuclides at the reference speed (portals) or collection interval (fixed) as required:

- Unshielded: ^{57}Co, ^{60}Co, ^{67}Ga, ^{99m}Tc, ^{131}I, ^{133}Ba, ^{137}Cs, ^{192}Ir, ^{201}Tl, ^{233}U, ^{235}U, ^{238}U, plutonium*, ^{241}Am, ^{237}Np.
- Natural materials: Natural sources (such as potash, granite and ceramic tile) will be used to test monitors for the ability to identify the isotopes ^{40}K, ^{226}Ra and ^{232}Th;
- Shielded by materials that are typical of inspected containers: ^{60}Co, ^{131}I, ^{133}Ba, ^{137}Cs, ^{192}Ir, ^{238}U, plutonium*, ^{237}Np.

More specific requirement is set by another program - Stand-Off Radiation Detection System (SORDS). The goal is to design a system for detection, identification, and localization of small radiation sources (1 mCi) at large distance (100 m) from a moving platform [81].

A high cost and a great demand for scintillators from passive systems developers lead to the of large size (400–500 mm length) NaI(Tl) or CsI(Na) scintillation crystals use for γ-quanta registration, which allow detecting masked fissile materials in a relatively short acquisition time at a distance.

2.4.2 Active Detection Systems

Such systems are commonly used for transmission radiography inspection. Active systems typically use an X-ray or gamma ray source to provide images of high-density and low-density materials in luggage, trucks or containers. Transmission radiography techniques may be useful to detect high Z materials that are often used in shielding. Many different sources are used for such radiography. The γ-ray radiography systems use ^{60}Co or ^{137}Ce as a radioactive source and a vertical tower of gamma detectors. The 1.25 MeV energy can penetrate through 15–18 cm of steel [82]. The X-ray radiography (including backscattering radiography) is similar to the γ-ray one. It uses a high-energy bremsstrahlung spectrum with energy in the 5–10 MeV range for large objects. Such X-ray systems can scan up to 30–40 cm of steel in vehicles moving with velocities up to 13 km/h. Muon tomography is a new technique that uses cosmic ray muons. Since muons are more deeply penetrating than X-rays, the scanner can be used to image thick and even shielded materials [83].

Active detection systems are under standards as well, see e.g., N42.40 – Standard for Evaluation and Performance of High-Energy, X- and γ-ray Interrogation Systems for Detection of Contraband.

The history of luggage inspection includes a few generations of X-ray scanners, starting from a planar metal shape inspection. The main point is to rapidly identify a suspect luggage in a few cubic meters large container moving across the inspection device. An important requirement for such a scanner is the highest possible throughput. The spatial resolution is related to the need to localize and possibly

to identify the suspect object in a large container [84]. The modern technique is usually based on a dual-energy 140 keV X-ray system [85]. After the X-rays pass through the item, they are picked up by the first detector. This detector then passes the X-rays on to a filter, which blocks out the lower-energy X-rays. The remaining high-energy X-rays hit the second detector. The computer compares the pick-ups of the two detectors to better represent low-energy objects, such as most organic materials.

Since different materials absorb X-rays at different levels, the image on the monitor lets the operator see distinct items inside the bag. These items are typically colored in the image, and based on the range of transmitted energies and represent one of three main categories: organic, inorganic or metal. Standard screening devises possess the ability to recognize shape (weapon, for example), separate materials with different density and Z_{eff}, i.e., to separate organic and non-organic materials. Advanced scanners have to provide separation even through different organic materials – explosives and food. Both materials consist of the same chemical elements like O, N, C, H. The main task is to find the combinations of elements that are typical of explosives. A deep analysis in [86] demonstrates specific areas of O-N rate that allows one to define the structure of organic materials as seen from Fig. 2.14. Multi-energy CT is the option to obtain better organic tissues discrimination at lower dose. Some methods allow us to determine Z_{eff} with the accuracy of about 5 % [87].

In addition to an X-ray system, airports also use larger volume and container scanners. These systems are basically larger versions of the X-ray system used for carry-on items. The main differences are higher speed and X-ray energy.

The modern standards require the use of computer tomography (CT) scanners. The technical solutions in this case are very similar to X-ray CT scanners, which are developed for medical applications. The scanner is able to calculate the mass and density of individual objects in a bag from the tomogram. If the object mass/density

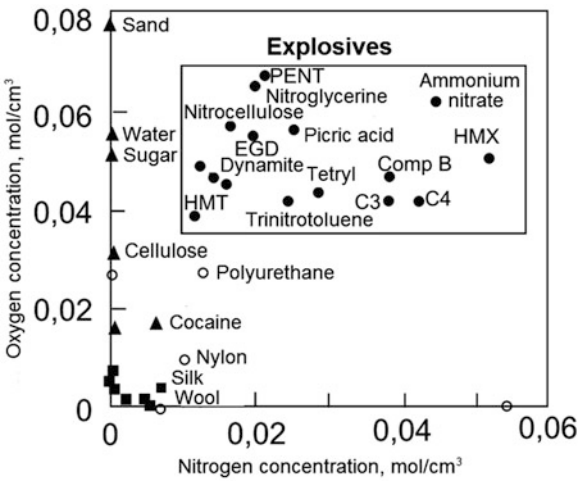

Fig. 2.14 Areas of O-N rates for explosive material verification

Table 2.5 Parameters of typical scintillators that are in use in security and medical CT scanning (99 % absorption for 120 keV)

Scintillator	Density (g/cm^3)	Thickness to stop 99 % (mm)	Relative light output	Emission band maximum	Primary decay (μs)	Afterglow (% at 3 ms)
$CdWO_4$	7.9	2.6	1	495	2, 15	<0.1
CsI:Tl	4.53	6.8	3.7	560	0.98	<5
ZnSe	5.27	6.4	3.5	610	1–3	<0.2
				640	30–50	
$Gd_2O_3:Eu^{3+}$	7.55	2.6	–	610	–	–
$(Y,Gd)_2O_3$: Eu	5.9	6.1	1.52	610	1000	5
Gd_2O_2S:Pr, Ce	7.34	2.9	1.8	520	2.4	<0.1
Gd_2O_2S:Tb (Ce)	7.34	2.9	1.8	550	600	≤0.7
La_2HfO_7:Ti	7.9	2.8	0.45	475	10	–
$Gd_3Ga_5O_{12}$: Cr	7.09	4.5	1.38	730	150	<0.1

falls within the range of a dangerous material, the CT scanner warns the operator of a potentially hazardous object. Let us note that CT scanners are slow compared to other types of baggage-scanning systems. The requirements for scintillators are very similar to those in medical **CT** (Table 2.5).

2.4.3 Neutron Activation Analysis for Security Systems

Active inspection (interrogation) techniques utilize both neutron and gamma ray sources and include nuclear resonance fluorescence, neutron and gamma ray multiplicity, neutron radiography, and neutron- and gamma ray-induced fission. These methods are based on the detection of either natural or induced characteristic neutron. Actually the most useful element-sensitive approaches are based on activation by a neutron source, either fast neutrons from the ^{252}Cf radioisotope or fast-thermal neutrons from a pulsed electronic neutron generator. The neutron-based methods are grouped into three categories: thermal neutron analysis (TNA), fast neutron analysis (FNA), and pulsed fast neutron analysis (PFNA). In these methods, neutron-induced reactions, such as elastic scattering, (n,γ), (n,p), (n, n′) and neutron activation are used [88]. Neutrons initiate reactions in certain elements, some of them producing characteristic γ-rays. Neutron activation analysis can verify up to 74 elements, depending upon the experimental procedure, with minimum detection limits ranging from 0.1 to $1 \cdot 10^6$ ng g^{-1}, depending on the element. Heavier elements have larger nuclei, therefore they have a larger neutron capture cross section and are more likely to be activated. Some nuclei can capture a

Table 2.6 Nuclear (n,γ) reactions of fast neutrons and light nuclei

Element	Reaction	Cross section (mb)	E_γ, MeV
C	(n,n'γ)	200	4.44
O	(n,n'γ)	750	6.13
N	(n, γ)	75	10.83
Cl	(n, γ)	4300	6.11
S	(n, γ)	520	5.42

number of neutrons and remain relatively stable, not undergoing transmutation or decay for many months or even years.

By allowing the fast neutrons to be thermalized between pulses, a large number of elements such as N, Cl, C, S, and O or their ratio in mixtures can be identified through the following (n,γ) reactions listed in Table 2.6.

One can see that the majority of nuclei, which are important for explosives identification, emit gamma-quanta in the energy range E_γ from 4 to 11 MeV. Many details of this method are used for security inspection, as described in ANSI standard N42.41 – "Standard for Evaluation and Performance of Neutron Interrogation Systems for Detection of Contraband".

In spite of the fact that heavy and high light yield crystals used in γ- spectrometry allow the registration of fast neutrons, most of the security inspection devices require the simultaneous presence of both γ- and neutron channels. In particular, the RPM standard [89] fixes the parameters of neutron registration. Fissile materials emit neutrons. Some nuclear materials, such as weapons usable plutonium-239, emit large quantities of neutrons, making neutron detection a useful tool to search for such contraband. Radiation Portal Monitors often use He-3 based detectors to search for neutron signatures. However, a global supply shortage of He-3 has led to the search for other technologies for neutron detection.

2.5 Physics of the Universe, Astrophysics, Nuclear Planetology

2.5.1 Dark Matter and Double Beta Decay Study

The latest trends in particle physics have raised interest in Dark Matter (DM) and Double Beta Decay (DBD) studies [90, 91]. The Invisible (dark) matter dominates in the Universe, but the experimental evidence is still lacking due to the problems with observation of WIMPs (Weakly Interacting Massive Particles). The main difficulty is the absence of a clear signature of the effect. Dark Matter searchers look for elastic nuclear recoils from WIMPs whose flux through the detector is estimated from cosmological models of the galactic halo. The cross section limit from the current experiments is about 10^{-44} cm^2 (spin independent). The 3rd generation experiments are expected to reach 10^{-48} cm^2. Such experiments will be performed in deep underground experiments to limit cosmogenically produced

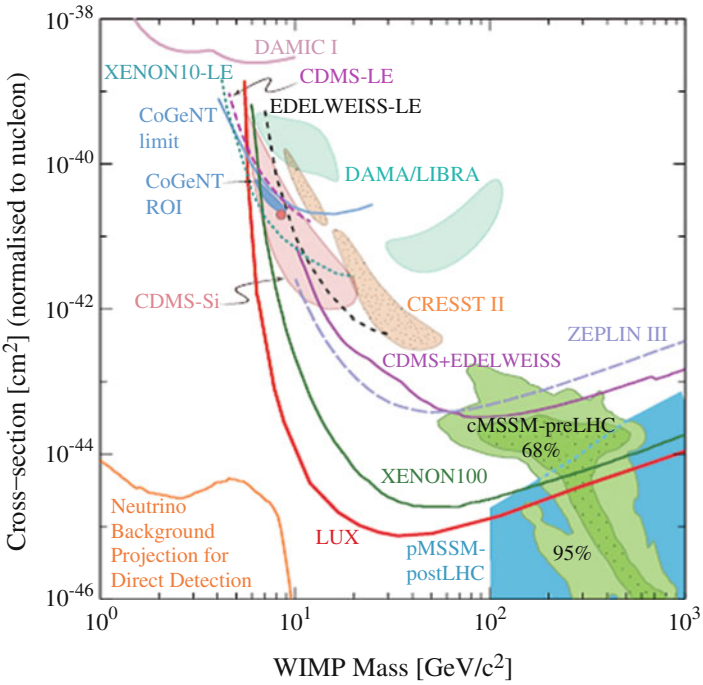

Fig. 2.15 WIMP cross sections (normalized to a single nucleon) for spin-independent coupling versus mass [91]

spallation neutron background. They will use different techniques to separate nuclear and electron recoils. The energy range of the WIMP inducing a nuclear recoil is below a few tens of keV. Figure 2.15 demonstrates the broad line of DM experiments based on different types of scintillation detectors.

The goal of DBD experiments is to observe the neutrinoless decay of a nucleus in order to determine the fundamental properties of the neutrino. The experiments are targeting to establish the mass of the neutrino in contrast to the mass difference which has been measured to date from the interactions of atmospheric, solar and reactor neutrinos. For this goal to be achieved, additional measurements in different isotopes would be necessary to remove uncertainties in these elements and to eliminate the possibility of contamination from an extremely very low intensity γ-ray emission at the exact energy of the neutrinoless DBD. There are several ton-scale neutrinoless Double-Beta Decay Experiment under development and construction right now.

The 3rd generation of experiments and projects are listed below. They claim for more and more specific radiation detectors [91]. For example, **LZD** Experiment is a 20-ton liquid xenon two phase Time Projection Chamber (TPC) utilizing direct scintillation and ionization to separate nuclear recoils. It would utilize a water shield and liquid scintillator veto system.

MAX is a two target observatory using 20 tons of depleted Ar in a two phase TPC and 6 tons of xenon (Xe), also in a two phase TPC. It should measure the WIMP mass by comparison of the recoil spectra.

GEODM consists of 300 5.1 kg Ge detectors. Separation of background is achieved by comparing ionization and phonon signals.

COUPP is an array of 32 500 kg bubble chambers utilizing CF_3I. This team has demonstrated an acoustic technique for identifying α-particles as well.

CLEAN is a single phase scintillation detector using 40 tons of Liquid Ar or Liquid Ne using Pulse Shape Discrimination to distinguish electrons from nuclear recoils.

Direct methods of WIMPs detection are based on registration of ionization or/and excitation of recoil nucleus in the material of the detector itself. There are many experiments directed to WIMPs registration and each of them uses different scintillators, like NaI(Tl) in DAMA/LIBRA [92], CsI(Tl) in KIMS [93], $CaWO_4$ in CRESST [94], $ZnWO_4$, $CaMoO_4$, CaF_2, LiF, BGO, $PbMoO_4$, $PbWO_4$, $MgWO_4$ in EURECA [95, 96], ZnSe in Lucifer [97].

These applications claim for specific particle detectors with a very low radioactive contamination, high energy resolution, very low energy threshold and the presence of certain elements (to study alpha, DBD) or variety of elements (for dark matter detectors). This initiated a construction of various new scintillators from low temperature gases, like LZ Dark Matter Experiment with 7 tons of liquid xenon detector [97], to organic (PPO-based multi tons liquid scintillator for Data Bay experiment [98]). But inorganic scintillators still remain the main option for the physics of universe study [90]. Some unique composition scintillators for such applications are listed in Table 2.7 [90].

The general scintillator claim for all rare-event application relates to extremely high level of radio purity. Radioactive contamination of the purest $ZnWO_4$ exceeds a reliable level by a factor of 20, CaF_2 – by a factor of 50, and $CaMoO_4$ – by a factor of 500 in the best purified samples. The most dangerous radionuclides for 2β experiments are ^{226}Ra and ^{228}Th with energies of β decay in the energy range up to 3270 keV and 4999 keV, respectively. Naturally occurring ^{40}K isotope is also nonreliable due to the high counting rate at 1461 keV.

The main problem for the crystal development for DBD experiments is a necessity of the enrichment of the crystals with different pure isotopes. Several high sensitivity studies of the double β decay processes were performed with isotope enriched samples: ^{40}Ca [99], ^{48}Ca [99], ^{70}Zn and ^{64}Zn [99], ^{106}Cd [100], ^{108}Cd and ^{114}Cd [100], ^{116}Cd [101], ^{130}Ba [102], ^{136}Ce and ^{138}Ce [103], ^{160}Gd [104], ^{180}W and ^{186}W [A102]. The development of ^{100}Mo containing crystals (this is one of the most promising candidates for 2β experiments for its high transition energy $Q2\beta = 3034.40 \pm 0.17$ keV) took several years. Finally three candidates ($CaMoO_4$, Li_2MoO_4, and $ZnMoO_4$) have been chosen from the list of molibdates. Very similar approach was used for $CdWO_4$ enriched with isotopes ^{106}Cd and ^{116}Cd.

Table 2.7 Radioactive contamination of scintillators (mBq/kg). Data for germanium crystals of HPGe detectors are given for comparison

Scintillator	Total α activity (U + Th)	^{228}Th	^{226}Ra	^{40}K	Particular radioactivity	References
$MgWO_4$	5700 ± 400	<50	<50	<1600		[106]
$CaWO_4$	400–1400	<0.2– 0.6	5.6 – 7	<12		[107–110]
$ZnWO_4$	0.2	0.002	0.002	<0.4	0.5 (^{65}Zn)	[111]
$CdWO_4$	0.3 – 2	<0.003– 0.039	<0.004	0.3 – 3.6	558 (^{113}Cd)	[101, 112–114]
					<3 – 30 (^{113m}Cd)	
$PbWO_4$	(53–79) 10^3	<13	<10		$(53–79) \cdot 10^3$	[115]
$PbWO_4$ (from ancient lead)					<4 (210Pb)	[116]
$PbMoO_4$					$(67–192) \cdot 10^3$	[117]
$CaMoO_4$	<10	0.04	0.13	<3		[118]
Li_2MoO_4	<300	<12	<21	170		[119, 120]
$ZnMoO_4$	73 ± 2	<(0.3–1.1)	<1.1 – 8.1			[121, 122]
YAG		70	170	3300		[109]
YAG:Nd	<20					[123]
$Li_6Eu(BO_3)_3$		<130	<70	<1500	949 (^{152}Eu)	[124]
					212 (^{154}Eu)	
BGO		<0.4 – 6	<1.2	<7	$7 – 3 \cdot 10^3$ (^{207}Bi)	[125, 126]
GSO(Ce)	40 – 217	2.3 – 100	0.3	<14	1200 (^{152}Gd)	[104, 127]
Lu_2SiO_5(Ce)					$3.9 \cdot 10^7$ (^{176}Lu)[a]	
NaI(Tl)	0.08 – 2.4	0.009 – 0.02	0.012 – 0.2	0.6		[128–130]
CsI(Tl)		0.0015 – 0.009	0.009 – 0.010		6 (^{134}Cs)	[131, 132]
					14 – 61 (^{137}Cs)	
$LaCl_3$(Ce)		<0.4	<34		$4.1 \cdot 10^5$ (^{138}La)	[133]
$LaBr_3$					$3.2 \cdot 10^5$ [b]	
LuI_3					$1.6 \cdot 10^7$ (^{176}Lu)[a]	
LiF(W)		<20	<20	<66		[134]

(continued)

Table 2.7 (continued)

Scintillator	Total α activity (U + Th)	^{228}Th	^{226}Ra	^{40}K	Particular radioactivity	References
CaF_2(Eu)	8	0.1 – 0.13	1.1 – 1.3	<7	10 (^{152}Eu)	[135, 136]
CeF_3	3400	1100	<60	<330		[103]
BaF_2		400	1400			[102]
Plastic scintillator		<0.00013				[137]
Liquid scintillator	$\approx 10^{-6}$	$(0.21 - 1.2) \cdot 10^{-6}$	$(0.043 - 6.3) \cdot 10^{-6}$	$<7 \cdot 10^{-5}$	0.3	[138–140]
		(^{232}Th)	(^{238}U)		(^{14}C)	
HPGe		$<2 \cdot 10^{-5}$	$<2 \cdot 10^{-5}$			[141, 142]

[a]Calculated value based on ^{176}Lu half life, isotopic composition and chemical formulas of LuI_3 and Lu_2SiO_5 compounds
[b]Calculated value based on ^{138}La half life, isotopic composition and chemical formula of $LaBr_3$ compound

It should be noted that some of the projects use cryogenic scintillating bolometers [105], which are extremely promising detectors thanks to high energy resolution and good particle discrimination. Scintillation at a very low temperature (10^{-3} K) has not been studied yet, i.e., such studies have to be the subject for luminescence investigation as well.

2.5.2 *Planetary Nuclear Spectroscopy*

Scientific problems of the origin and evolution of planetary bodies such as planets, their satellites and asteroids gain importance with our expansion in the solar system. Their spatial distribution in terms of concentrations of elements is an important clue for understanding the planetary history and evolution. The measurements of γ-rays, X-rays and neutrons emitted from the planet surface are the main abundant source of major elements and naturally radioactive γ-ray emitters. Neutron spectroscopy can provide the maps of hydrogen- and carbon-containing compounds.

Remote observations conducted during planetary missions have provided global information about the elemental and mineralogical composition of planetary surfaces. The main principles and methods of nuclear planetology (spectroscopy, nuclear planetary instruments, the nature of observational results) are described in [143].

Galactic cosmic rays are mainly high-energy protons (p) smashing the atoms from the top surface of atmosphereless bodies (Fig. 2.16). This produces a shower of secondary particles, which include neutrons (n). These neutrons then undergo successive collisions with atoms and produce gamma rays (γ) via inelastic scattering and radiative capture. Gamma rays can also be produced by the decay of natural

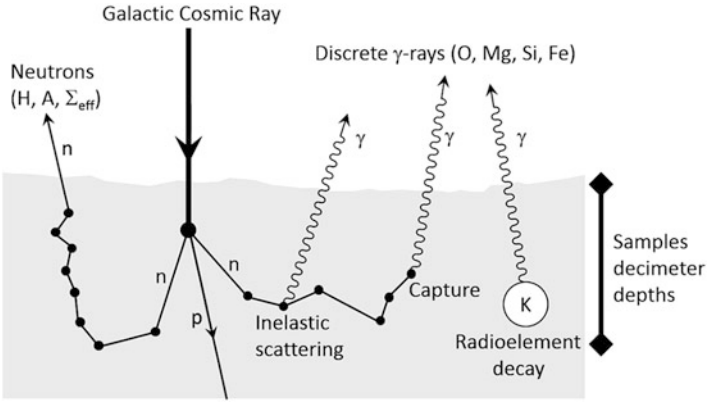

Fig. 2.16 Scheme of neutron and γ-ray production processes on the surface of planetary bodies [147]

radionuclides, such as K, Th and U. The spectrum of the gamma rays is the subject for analysis to determine the concentration of the detected elements. For example, important rock-forming elements include O, Mg, Si, and Fe.

Planetary spectroscopy requires high sensitivity γ-ray and neutron detection. The requirement for high efficiency claims for large-volume detectors. The most typical solution is high-purity germanium (HPGe) detector [144, 145]. But there are many cases when scintillator-based detectors are also efficient [146, 147]. Detectors must have low self-activity/noise levels [146]. For example, gamma rays produced from the decay of radio-lanthanum in the scintillator lanthanum bromide ($LaBr_3$) can obscure γ-ray emissions from the Moon [149].

This application is unique and the cost of the scintillator is generally not a too important issue.. This is the reason for selecting the best spectroscopy grade materials like $LaBr_3$ [147, 148, 150] or $CeBr_3$ [151].

2.5.3 *Astrophysics*

Space physics makes use of scintillators in two different locations: low orbit satellites and space or interplanetary missions. The low orbit satellites are shielded by the Earth's magnetic field, relaxing therefore the requirement for radiation hardness of the scintillation material. Most of the scintillation materials can be used depending on the energy range of the detected γ-radiation. However, the payload limits the size of such detectors and not too dense materials are sometimes selected to reduce the weight.

In the interplanetary space, the sun wind from charged particles strongly influences the detecting properties of the scintillation material. Although the studies in this domain are still not systematic, one can state that relatively light, fast and bright scintillators are the most prospective ones for space missions in the future and that $LaBr_3$, YAP and $CeBr_3$ are likely to become the scintillators of choice.

The list of the main projects performed in gamma astrophysics from the beginning of the 90s is given in Fig. 2.17. Most of the current data on cosmic γ-sources have been accumulated from different gamma telescope measurements. The main peculiarity of these measurements was based on the design of position-sensitive telescopes, which is not a simple task. Two classes of position sensitive devices have been developed in the last decades. These designs use continuous geometries of scintillation crystal or pixilated detector [152].

Scintillation detectors with a continuous crystal are generally based on Anger camera logics as for nuclear medicine gamma cameras. An example of such gamma camera is the SIGMA mission on GRANT, where a 12.5 mm thick NaI(Tl) crystal is viewed by 61 hexagonal PMT through a 12.5 mm thick glass. The energy resolution of about 10 % FWHM is achieved at 120 keV with a position resolution of 4 mm at this energy. The detector is surrounded by an active CsI(Tl) veto.

The use of an array of small discrete detectors offers an alternative to continuous crystal detectors. This design uses the same reconstruction principle as HEP

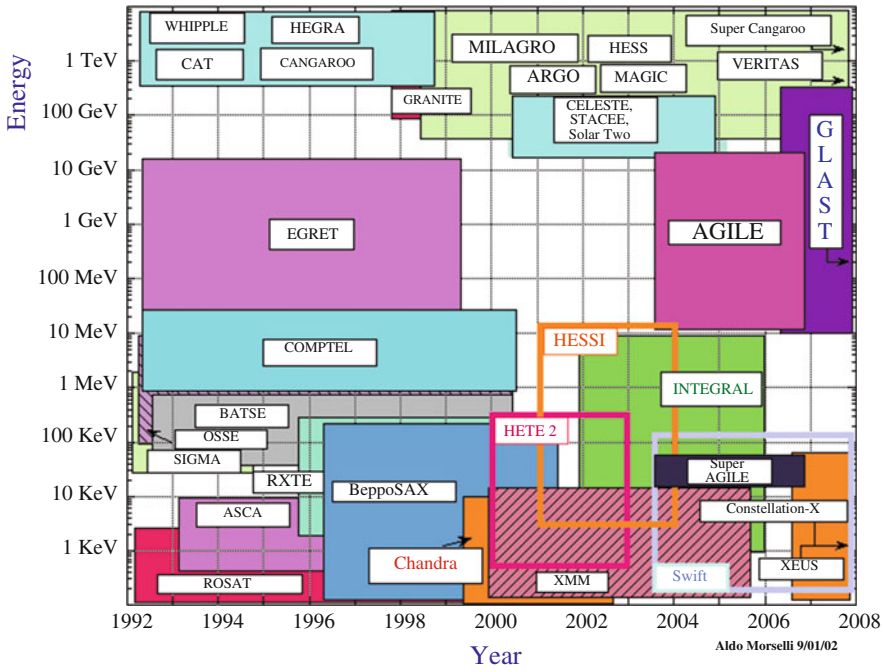

Fig. 2.17 List of the main projects for gamma astrophysics from the beginning of the 1990s [155]

calorimeters (see Sect. 2.1) or some medical cameras. An example of gamma telescope based on pixilated detector is the imager of the INTEGRAL detector [154, 155]. The INTEGRAL is made of 3 layers of hexagonal CsI(Tl) scintillation bars. There are three planes with 2880 scintillation elements coupled to silicone photodiodes. This arrangement provides good imaging and sensitivity in the 50 keV – 10 MeV range. The BGO scintillators are used as veto shields as in several other detectors. This includes 38 bars with dimensions $20 \times 90 \times (310–345)$ mm.

The investigations of the high-energy component of cosmic γ-radiation are of crucial importance to understand the emission mechanisms of galactic sources. This is the goal of several experiments e.g. of the GILDA mission [78].

High-energy γ-ray astrophysics has greatly developed at the beginning of the 90s, following the results of the EGRET (Energetic Gamma Ray Experiment Telescope) experiment [156]. The satellite observations have brought more detailed data about the well-known γ-ray sources, but have also led to the discovery of the new ones, both galactic and extragalactic, especially active galactic nuclei and gamma bursts.

The most serious problem affecting the EGRET telescope is the decrease of the detection efficiency at high energies due to the use of anticoincidence counters placed around the detector.

The objective of EGRET was to make a major advance in high energy (20 MeV to about 30 GeV) γ-ray astrophysics using a γ-ray telescope with more than an order

of magnitude greater sensitivity and better angular and energy resolution than the previous instruments. The study of the γ-ray sky reveals the sites of the most energetic interactions occurring in astrophysics. Because these interactions are generally associated with dynamic, non-thermal processes in nature, γ-ray astrophysics provides an excellent opportunity to learn about the evolution of the universe. In addition, since high-energy gamma-rays have a low interaction cross section, they have a very high penetration capability and can reach the Earth from any part of the Galaxy or universe.

The EGRET detected γ-rays in the 20 MeV – 30 GeV range. It had a very large field of view, approximately 80° in diameter, although the instrument point-spread function and the effective area degraded significantly beyond 30° off-axis. The effective area on-axis was more than 1000 cm^2 between 100 MeV and 3 GeV. The angular resolution was strongly energy-dependent, with a 67 % confinement angle of 5.5° at 100 MeV, falling to 0.5° at 5 GeV on axis; bright γ-ray sources can be localized with approximately 10' accuracy. The energy resolution of the EGRET was 20–25 % over most of its range of sensitivity. The arrival times of photons were recorded with approximately 50 μs accuracy. The instrument used a multilevel thin-plate spark chamber system to detect γ-rays by the electron-positron pair production process. A calorimeter using NaI(Tl) is placed beneath the instrument to provide a good energy resolution over a wide dynamic range. The energy of the γ-ray is determined from the measurements made in an eight radiation-length thick, 76 cm × 76 cm square NaI(Tl) scintillator crystal below the lower time-of-flight scintillator plane. The NaI(Tl) detector is covered with a plastic scintillator anticoincidence dome to prevent triggering-on events not associated with γ-rays.

The first scintillators for gamma telescopes were relatively simple and did not trigger large developments on scintillators. But this situation was progressively modified by the higher requirements for space physics experiments for a new generation of scintillators for space started with the GLAST project (Global Large Area Space Telescope) [158, 159].

The GLAST Mission is a part of NASA's Office of Space and Science Strategic Plan launched in 2006. The GLAST is a new generation high-energy γ-ray observatory designed to study celestial γ-ray sources in the energy band extending from 10 MeV to more than 100 GeV.

GLAST has more advanced missions and has to cover several important directions in astrophysics:

1. Understand the mechanisms of particle acceleration in pulsars and other space sources.
2. Create a precise map of γ-ray source in the sky: unidentified sources and diffuse emission.
3. Determine the high-energy behavior of γ-ray bursts and transients.
4. Probe dark matter and early universe.

The observation of γ-ray pulsars is an important tool to understand supermassive black holes through jet formation and evolution studies and to set constraints on the star formation rate through photon-photon absorption over

extragalactic distances. There is also a possibility to observe mono-energetic -ray "lines" above 30 GeV from super-symmetric dark matter interactions, to detect decays of relics from the very early universe, such as cosmic strings or evaporating primordial black holes; or even to use γ-ray bursts to detect quantum gravity effects.

GLAST has a field of view about twice as wide as (more than 2.5 steradians) and a sensitivity about 50 times as large as those of EGRET at 100 MeV and even more at higher energies. Its 2-year limit for source detection in an all-sky survey is $1.6 \cdot 10^{-9}$ photons $\mathrm{cm}^{-2}\ \mathrm{s}^{-1}$ (at energies greater than 100 MeV). This allows one to localize sources with a position accuracy of 30 arc seconds to 5 arc minutes.

The calorimeter of GLAST measures the energy of the cosmic γ-rays. The CsI (Tl) bars, arranged in 16 flat towers, give both the longitudinal and transverse information about the energy deposition pattern. Once a gamma ray penetrates through the anticoincidence shield, the silicon-strip tracker and the lead converter planes, it is then absorbed in the cesium-iodide calorimeters. This produces scintillation in the cesium-iodide crystal, and the resultant light flash is photoelectrically converted to a voltage pulse. This voltage signal is then digitized, recorded and relayed to earth by the spacecraft's onboard computer and telemetry antenna. Cesium-iodide blocks are arranged in two perpendicular directions to provide additional positional information about the shower [159]. It was necessary to develop a position-sensitive detector from a unique long scintillation crystal.

Long scintillator crystals used in HEP projects require that the light output be as uniform as possible along the scintillator. The light yield uniformization was employed in many experiments using different techniques (painting the BGO crystals for the L3 experiment, depolishing one lateral face for the CMS PWO crystals, etc.). In the case of the 6624 CsI(Tl) scintillators of the electromagnetic calorimeter BELLE (KEK) [157], a light non-uniformity of less than 7 % along the 300 mm length of the crystal was achieved. Such approach was also used for BaBar CsI(Tl) scintillator treatment to unify the light output to 6 % [153].

Contrary to the HEP case, surface treatment can be applied to long crystals to induce on purpose a non-uniform distribution of the light output [158]. Figure 2.18 describes schematically the principle of position sensitivity of a long length scintillator and conditions to be fulfilled to achieve such a property. This approach works particularly well for a large aspect ratio (small cross section as compared to the length).

Such light output distribution can be easily tested in the same way as it is done for systematic quality control of HEP crystals. For 20 mm × 20 mm × 400 mm CsI (Tl) crystals with unpolished side surfaces, Fig. 2.19 shows the characteristic pulse height spectrum with a ^{22}Na collimated source placed at different positions along the crystal.

The position resolution values for detectors of different length have been calculated according to Eq. (2.3). The position of the collimated source of ionizing particles z can be determined by the measured value of the light yield c. The accuracy δz of the source position determination is defined by the value of the pulse height resolution (PHR) of the detector R and the slope α of function $c(z)$ at the point of measurement:

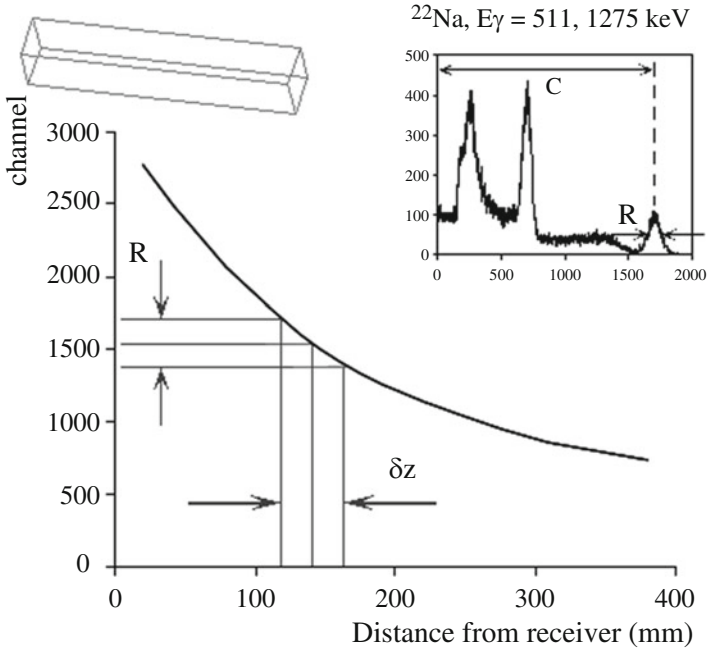

Fig. 2.18 Principle of position determination on a long scintillation crystal. The side surface of the detector is depolished to induce a strong light collection dependence on the emission point position. The accuracy of the position determination δz is defined by the light yield c, the pulse height resolution R, and the slope of the curve at the point of interaction

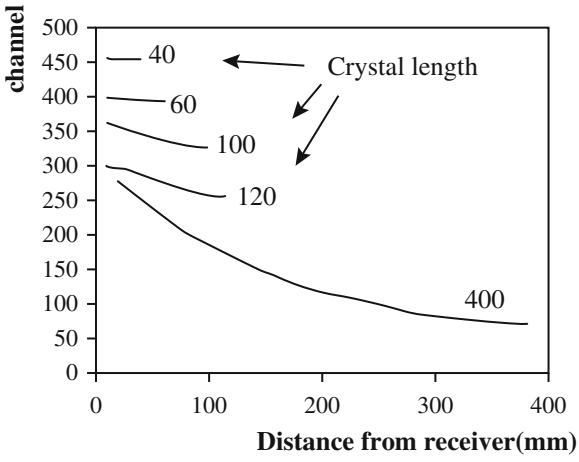

Fig. 2.19 Light yield distribution in scintillators of different lengths. Reflective properties of the detector surface, its coating and parameters of signal amplification are kept unchanged, so the comparison can be made. If detector shortens, average light yield becomes higher [158]

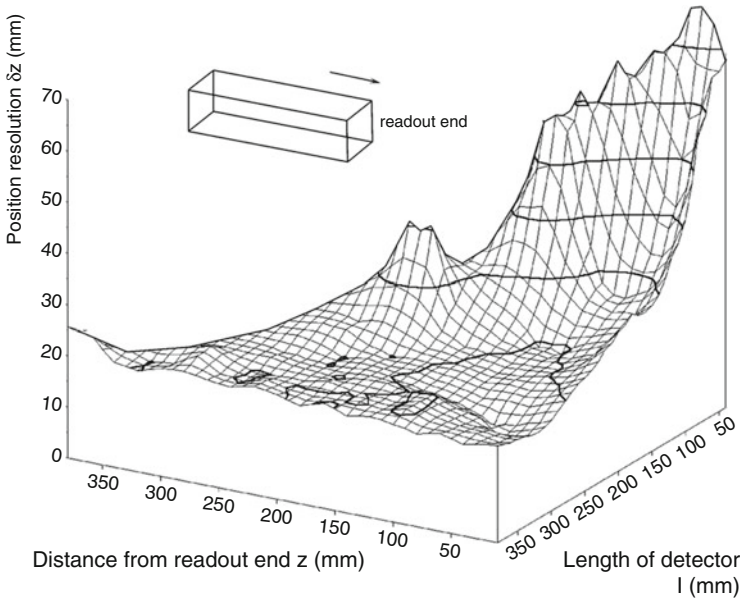

Fig. 2.20 Position resolution of detectors of different lengths from Eq. (2.3)

$$tg\alpha = \lim_{\Delta z \to 0} \frac{\Delta c}{\Delta z}, \delta z = c\frac{R}{tg\alpha} \tag{2.3}$$

To achieve a better position sensitivity one needs to improve the light yield and energy resolution of the detector and to keep the $c(z)$ distribution as steep as possible. These requirements are somewhat contradictory. In practice a good determination of the position of the γ-conversion point in a crystal results from a compromise between these parameters as a function of the state of the art for the light collection procedure.

The dependence of the position resolution $\delta z(z, l)$ on the detector length and position of the collimated source is shown in Fig. 2.20.

It is seen that the position resolution remains more or less constant over the whole volume of the detector when its length varies in the range 200 to 380 mm. Equation (2.3) can be rewritten in a form giving more physical sense to this phenomenon:

$$\delta z = \frac{R}{(\ln c)_z'} \tag{2.4}$$

It was found that the optimal cross section/length ratio is 1:10 or less. But the total size of the detector is restricted by the attenuation factor K of the light propagating along the crystal. In the example given $\exp(-l \cdot K) = 0.82$. As the scintillator becomes longer the need for a higher transparency increases.

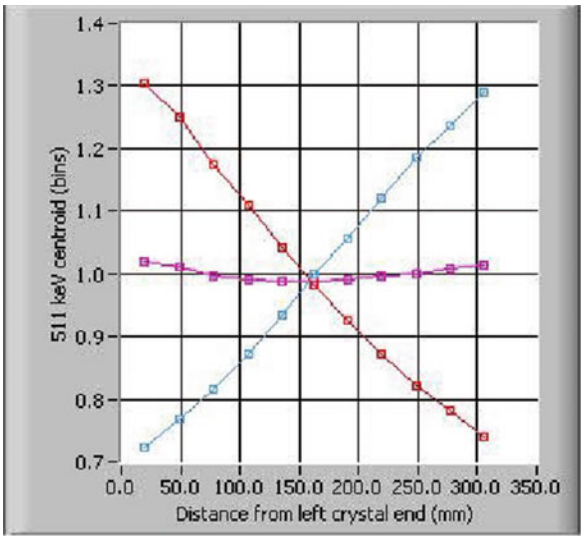

Fig. 2.21 CsI(Tl) crystal light output distribution for the GLAST gamma telescope assembly. Oblique curves show the typical light output distribution along the scintillator as seen from each end. The horizontal curve shows a good uniformity of the mean value within 5 %

The position resolution can be improved by combining signals from two photodetectors coupled to opposite ends of the crystal. Figure 2.21 shows the light output distributions for the GLAST type position sensitive detector [158].

Two position dependant curves are obtained from the light distribution measurements from opposite ends of the crystal. The mean value is uniform within 5 %.

There are more and more examples of crystal detectors used for astrophysics experiments and this trend should continue with the growing interest in γ-ray astrophysics.

2.6 Well and Mud Logging

Oil well logging has been known for many years. It provides an oil and gas well driller with information about the particular earth formation being drilled. In conventional oil well logging, during well drilling and/or after the well has been drilled, radiation detectors and a radiation source, usually called tool, may be conveyed into the borehole and used to determine one or more parameters of interest for the formation. Well logging progress also followed the progress in the development of scintillation materials. The first generation of the tools was able to measure natural radioactivity. These tools provide a log of total gamma ray intensity as well as spectral gamma ray measurement. This measurement was important to discriminate the presence and contribution of Potassium (K), Thorium (Th) and Uranium (U). The intensity of the measured radiation provides an indication of the type of rock penetrated by the wellbore. NaI(Tl) crystals still dominate such measurements. Their use is an effective way to identify the variation of

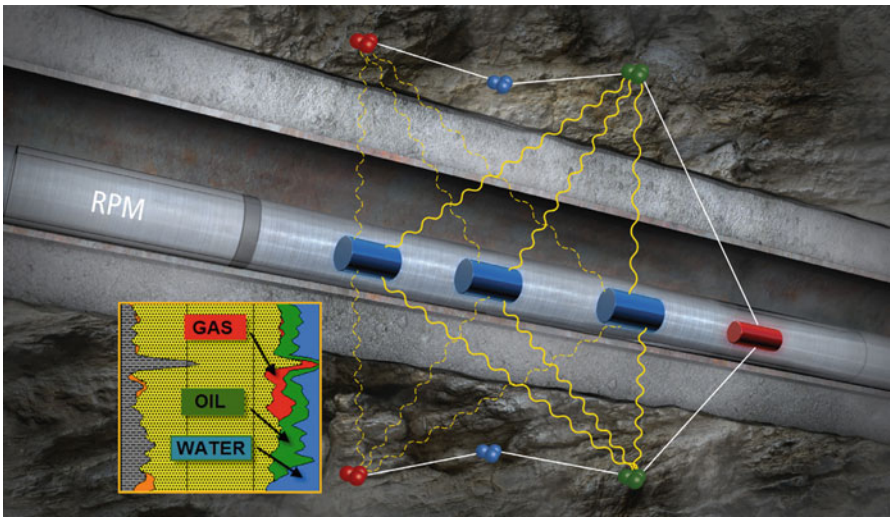

Fig. 2.22 Sketch of RPM tool for active well logging. Small *red* cylinder schematically indicates fast neutron source, *blue* cylinders-diferent detectors. *Red*, *green* and *blue* balls shows different type of the gamma-quanta emitting nuclei. Inset indicators presence of gas, oil and water measured along the well (Courtesy of Baker Hughes)

lithology along the well and to distinguish the reservoir zones from non-reservoir or shale zones, since radioactive elements tend concentrate in the shales, whereas the elements in carbonate and sandstone layers tend to be less radioactive. Moreover, different formation types contain different quantities of naturally occurring radioactive elements. Particularly, U/Th and U/K ratios correlate with oil saturation of the formation. The organic carbon content creates a reducing environment, beneficial for U accumulation [160]. One of the frequently used tools is Nautilus Ultra GR/SL^{TM} (Baker Hughes) which is able to operate under extreme high-pressure/high-temperature conditions, while measuring the natural radioactivity of the formation being surveyed.

The next generation of wireline tools are being used in well radiation sources to expose the formation. The typical construction of Reservoir Performance Monitor (RPM), the modern tool which includes the neutron source is shown in Fig. 2.22.

The downhole tools include this radiation source and one or more detectors placed into one or more detector chambers. The radiation source is either a 14 MeV neutron gun, a γ-ray source, or an X-ray source. The detectors are used to detect natural and induced radiation from the formation. Modern tools allow solving several important problems. First, reducing the reservoir uncertainty in petrophysical modeling, especially when the reservoir heterogeneity increases. Second, identification of shale zones and their characterization for total organic carbon or kerogen present in the reservoir.

Fast neutrons initiate reactions in the formation, as described in Table 2.6. Hence, the tool having a 14 MeV source is usually equipped with a thermal neutron counter and a γ-quanta detector. In many cases, ^{3}He based counters are used to detect thermal neutrons in the tool. An alternative is to apply neutron-sensitive glass enriched with ^{6}Li. There is a set of ^{6}Li containing glasses at the market [161]. One of the widely used scintillation glasses is GS20. It provides registration of thermal neutrons with the counting rate one order of magnitude higher than that of ^{3}He counters y. In spite of that the density of the glass is low, about 2.5 g/cm^3. It becomes sensitive to γ-quanta initiated by neutrons in the formation. Thus, the search for materials with better neutron/γ-quanta discrimination becomes an important task. From that point of view, the recently recognized Cs_2LiYCl_6: Ce^{3+} [162, 163] scintillation crystal can open an opportunity for more reliable pulse shape discrimination of thermal neutrons.

Requirements for the scintillation materials to detect γ-quanta in the tools are the same as described in paragraph Sect. 2.4.3. They have to possess high stopping power and be bright and desirably fast. However, due to a limited space in the tool and dimensions of the well, the scintillation detector cannot be packed into the envelop with high thermo-insulation. Therefore, moderate deterioration of the crystal's light yield with increasing temperature in the range from 20 to 175 °C becomes critically important. From that point of view, YAP:Ce, $LaBr_3$:Ce and $CeBr_3$ are the scintillators of choice. The Pr^{3+} activated crystals demonstrate even better LY(T) dependence. Trivalent praseodymium has some advantageous over a cerium activator; its luminescence radiating time is two times shorter than that of cerium in the same compounds due to a systematic shift (−1.5 eV) of Pr^{3+} $f \rightarrow d - f$ transitions to the UV range relatively to the same transition of a trivalent Ce ion [164, 165]. Moreover, the energy difference between the radiating *4f5d* state and the next level of f configuration is larger than 1.2 eV (10000 cm^{-1}) in the majority of crystals where the interconfiguration luminescence of Pr^{3+} ions exists. Both features make Pr^{3+} ion radiating transitions less dependent on the temperature. However, this ion has a more complicated structure of energy levels than the Ce^{3+} ion. Among Pr-doped materials, $YAlO_3$ and $Lu_3Al_5O_{12}$ crystals doped with Pr^{3+} ions showed very good LY(T) dependence, making their use in downhole measurements prospective [166–169, 170]. However, both crystals have their interconfiguration luminescence in the UV range, making their use with ordinary PMT difficult or even worse with novel silicon PMT (SiPM).

The requirements for scintillation materials are even stricter when the tool is used while drilling. This approach allows shortening the time of drilling and exploration, and gives an opportunity to control the direction of drilling. So, Logging While Drilling (LWD) tools become a powerful instrument way for in-earth navigation. However, the tools' detectors are under vibration while drilling. Therefore, the mechanical stability of the scintillation material and its resistance to cracking are crucially important requirements for LWD application. Mechanically hardened NaI(Tl) is one of the possibilities to meet this requirement.

Nevertheless, tool size restrictions limit the detector performance:

- Real-time data collection in logging-while-drilling mode requires instruments with complex design, vibration and thermal stabilization. This increases the instruments' cost.
- Gamma well logging in integral detector mode (most widely used until now) does not provide information on the content of individual chemical elements.
- Model well is needed for precise instrument calibration.

Another possibility to characterize the well is to evaluate the drill cuttings extracted from the well. Mud logging is vital for rig safety and gives the first indication of the potential success of the well.

Gas saturation of the drilling mud, as well as different parameters of drill cuttings, are usually analyzed on-site. Drill cuttings are usually observed visually and by using an optical microscope to determine the formation lithology, the grain size, the color and porosity, and the basic fluorescence characteristics [171, 172, 173]. This gives only a limited set of data. The drill cuttings are separated from a drilling mud.

Similarly to well logging, the spectrometry of naturally containing K, U, and Th is one of the targets for measurements. However, there are no limits for the detector dimensions. A sample (appr. 100 g) of drill cuttings is weighted and placed into the measurement camera of a highly sensitive gamma-spectrometer (shielded from the background radiation). The gamma-spectrum is recorded and used for precise determination of K, Th, and U content in the sample (down to 2–3 ppm for U and Th).

A unique lower limit of measured concentrations has been achieved in the routine instruments having NaI(Tl) crystals with volume up to 5 litres. This allows one to refine the existing correlations and to ascertain new ones for a more precise characterization of oilfields.

References

1. Derenzo SE, Moses WW, Huesman RH et al (1993) Quantification of brain function: tracer kinetics and image analysis in brain PET. Elsevier Science Publishers, Amsterdam, p 25
2. L3 Collaboration, Adeva B et al (1990) The construction of the L3 experiment. Nucl Instr Meth Phys Res A289:35–102
3. Birks JB (1951) The specific fluorescence of antracene and other organic materials. Proc Phys Soc (London) Letters to the Editor, pp 365–366
4. Hofstadter R (1948) Alkali halide scintillation counters. Phys Rev 74:100–101
5. Oreglia M et al (1982) Study of the reaction psi – gamma gamma. J/psi Phys Rev D 25:2295–2277
6. Kubota Y et al (1991) The CleoII detector. CLNS 91/1122
7. Amsler C (1998) Proton-antiproton annihilation and meson spectroscopy with the Crystal Barrel. Rev Mod Phys 70:1293
8. Ray RE (1994) The KTeV pure CsI calorimeter. In: Proceeding fifth international conference on calorimetry in high energy physics. World Scientific, Hackensack, pp 110–114

9. The Belle Collaboration (1995) Technical design report. KEK Report, Stanford, pp 95–1
10. The BaBar Collaboration (1995) BaBar technical design report. SLAC-R-95-457. KEK Report, Stanford
11. Novotny R, Riess R, Hingmann R et al (1987) Detection of hard photons with BaF_2 scintillators. Nucl Instr Meth Phys Res A262:340–346
12. GEM Letter of Intent, SSCL SR-1184, November 1991
13. CMS Technical Proposal, CERN/LHCC 94–38, December 1994
14. L3P Letter of Intent, CERN/LHCC 92–5 (1992)
15. ALICE Collaboration Technical Proposal, CERN/LHCC/95-71 (1995)
16. R&D Proposal for the study of new fast and radiation hard scintillators for calorimetry at LHC: Crystal Clear Collaboration, CERN/DRDC P27/91–15, project RD-18
17. Lecoq P, Li PJ, Rostaing B (1991) BGO radiation damage effects: optical absorption, thermoluminescence and thermoconductivity. Nucl Instr Meth Phys Res A300:240–258
18. Annenkov A, Auffray E, Borisevich A et al (1999) Suppression of the radiation damage in lead tungstate scintillation crystal. Nucl Instr Meth Phys Res A426:486–490
19. Ilmas ER, Liidya GG, Lushchik CB (1965) Photon multiplication in crystals. Opt Spect 18:255–263 (in Russian)
20. Birks JB (1951) Scintillation from organic crystals: specific fluorescence and relative response to different radiations. Proc Phys Soc A64:874–877
21. Birks JB (1951) The Specific Fluorescence of Antracene and Other Organic Materials. Proc Phys Soc (London), Letters to the Editor 84: 364–365
22. Dorenbos P, de Haas JTM, van Eijk CWE (1995) Non-proportionality in the scintillation response and the energy resolution obtainable with scintillation crystals. IEEE Trans Nucl Sci 42:2190–2202
23. Rooney BD, Valentine JD (1997) Scintillator light yield nonproportionality: calculating photon response using measured electron response. IEEE Trans Nucl Sci 44:509–516
24. Pringle RW, Standil S (1950) The γ-rays from neutron-activated gold. Phys Rev 80:762–763
25. Aitken DW, Beron BL, Yenicay G et al (1967) The fluorescent response of NaI(Tl), CsI(Tl), CsI(Na), and CaF (Eu) to X-rays and low energy gamma rays. IEEE Trans Nucl Sci NS-14:468–477
26. Rooney BD, Valentine J (1997) Scintillator light yield nonproportionality: calculating photon response using measured electron response. IEEE Trans Nucl Sci 44:509–516
27. Uchiyama Y, Kouda M, Tanihata C et al (2001) Study of energy response of $Gd_2SiO_5:Ce^{3+}$ scintillator for the ASTRO-E hard X-ray detector. IEEE Trans Nucl Sci 46:379–384
28. Moses WW (2002) Current trends in scintillator detectors and materials. Nucl Instr Meth Phys Res A487:123–128
29. Menghesha W, Taulbee TD, Rooney BD et al (1998) Light yield nonproportionality of CsI (Tl), CsI(Na), and YAP. IEEE Trans Nucl Sci 45:456–641
30. Menghesha W, Valentine JD (2000) A technique for measuring scintillator electron energy resolution using the compton coincidence technique. In: Mikhailin VV (ed) Proceeding of the fifth international conferences on inorganic scintillators and their applications, SCINT99. Moscow State University, Moscow, pp 173–178
31. Balcerzyk M, Moszynski M, Kapusta M (2000) Energy resolution of contemporary scintillators. Quest for high resolution, proportional detector. In: Mikhailin VV (ed) Proceeding of the fifth international conferences on inorganic scintillators and their applications, SCINT99. Moscow State University, Moscow, pp 167–172
32. Balcerzyk M, Klamra W, Moszynski M et al (2000) Nonproportionality and temporal response of ZnSe:Te scintillator studied by large area avalanche photodiodes and photomultipliers. In: Mikhailin VV (ed) Proceeding of the fifth international conferences on inorganic scintillators and their applications, SCINT99. Moscow State University, Moscow, pp 571–576
33. Baryshevsky VG, Korzhik MV, Moroz VI et al (1991) $YAlO_3$:Ce – fast-acting scintillators for detection of ionizing radiation. Nucl Instr Meth Phys Res B58:291–293

34. Korzhik MV, Misevich OV, Fyodorov AA (1999) $YAlO_3$:Ce scintillators: application for X- and soft γ-ray detection. Nucl Instr Meth Phys Res B72:499–501
35. Baryshevsky VG, Korzhik MV, MorozVI et al (1992) YAlO3:Ce scintillator for the detectors of ionizing radiation. IET 3: 86–92 (in Russian)
36. Baryshevski VG, Korzhik MV, Bogatko AV et al (1992) Scintillator YAlO3:Ce3+ fro the α-particles spectrometry. Izvestia AN BSSR Physics 2:5 (in Russian)
37. Kachanov VA, Rykalin V, Korzhik M et al (1992) Light source for energy stabilization of calorimetric detectors based on photodetectors. Nucl Instr Meth Phys Res A314:215
38. Drobyshev GY, Korzhik MV, Missevitch OV et al (1993) An application of YAlO3:Ce scintillator to detect soft γ-quanta. IET 3:176 (in Russian)
39. De Notaristefani F, Pani R, Scopinaro F et al (1995) First results from a YAP:Ce gamma camera for small animal studies. IEEE Trans Nucl Sci 43:3264–3271
40. Korzhik M, Missevitch O, Kholmetskii AL et al (1994) YAlO3:Ce scintillation detector for transmission Mossbauer spectroscopy. 4-th Seeheim workshop on Mossbauer spectroscopy Abstracts Seeheim, Germany Institute fur Anorganische und Analiytiche Chemie, der Jogannes Gutenberg Universitat, Mainz, p 126
41. Fedorov AA, Kholmetskii AL, Korzhik M et al (1994) High-performance transmission Mossbauer spectroscopy with YALO3:Ce scintillation detector. Nucl Instr Meth Phys Res B88:462–464
42. Kobayashi M, Shinkawa T, Sato T et al (1994) YALO3:Ce-Am light pulsers as a gain monitor for undoped CsI detectors in a magnetic field. Nucl Instr Meth Phys Res A337:355–361
43. Missevich O (2000) Increase of the productivity and precision of Mossbauer measurments in transmission and scattering geometry. Ph.D. thesis, Minsk, 2000, p 150 (in Russian)
44. Moszynski M (2003) Inorganic scintillation detectors in γ-rays spectrometry. Nucl Instr Meth Phys Res A505:101–110
45. Globys ME, Grinev BV (2000) Inorganic scintillators. New and traditional materials. Acta, Kharkov (in Russian)
46. Anger HO (1958) Anger camera for nuclear medicine. Rev Sci Instr 29:27–45
47. Moses WW (2000) Scintillator requirements for medical imaging. In: Mikhailin VV (ed) Proceeding of the fifth international conferences on inorganic scintillators and their applications, SCINT99. Moscow State University, Moscow, pp 11–21
48. Blasse G (1994) Scintillator materials. Chem Mater 6:1465–1475
49. Greshkovich C, Duclos S (1997) Ceramic scintillators. Annu Rev Mater Sci 27:69–88
50. Deych D, Dobbs J, Marcovici S, Tuval B (1996) Cadmium tungstate detector for computed temograhy. In: Dorenbos P, van Eijk CWE (eds) Inorganic scintillators and their application. Delft University Press, pp 36–39
51. Kinloch DR, Novak W, Raby P, Toepke I (1994) New developments in cadmium tungstate. IEEE Trans Nucl Sci 41:752–754
52. Yoshida M, Suzuki A, Uchida Y et al (1988) Application of Gd_2O_2S ceramic scintillator for X-ray solid state detector in X-ray CT. Jap J Appl Physics 27:L1572–L1575
53. Rossner W, Grabmaier BC (1991) Phosphors for X-ray detectors in computed tomography. J Lumin 48–49:29–36
54. Kostler W, Winnacker A, Rossner W, Grabmaier BC (1993) Effect of Pr-codoping on the X-ray induced afterglow of (Y, Gd)2O3:Eu. J Phys Chem Solids 56:907–913
55. Cherepy NJ, Payne SA, Asztalos SJ, Hull G, Kuntz JD, Niedermayr T, Pimputkar S, Roberts JJ, Sanner RD, Tillotson TM, van Loef E, Wilson CM, Shah KS, Roy UN, Hawrami R, Burger A, Boatner LA, Choong WS, Moses WW (2009) Scintillators with potential to supersede lanthanum bromide. IEEE Trans Nucl Sci 56:873–880
56. Cherepy NJ, Seeley ZM, Payne SA, Beck PR, Drury OB, O'Neal SP, MoraleS Figueroa K, Hunter S, Ahle L, Thelin PA, Stefanik T, Kindem J (2013) Development of transparent ceramic Ce-doped gadolinium garnet gamma spectrometers. IEEE Trans Nucl Sci 60:2330–2335

57. Levin CS, Habte F, Foudray A (2004) Methods to extract more light from minute scintillation crystals used in an ultra-high resolution positron emission tomography detector. Nucl Instr Meth Phys Res A527:35–40
58. Wieczorek H, Frings G, Quadfield P et al (1995) CsI:Tl for solid state X-ray detectors, Proc. In: Dorenbos P, van Eijk CWE (eds) Inorganic Scintillators and Their Applications, Delft University Press, pp 547–554
59. Cho G, Lee KS, Kim DK, Joo KS (1999) Annealing effect on optical emission properties of pure and Na doped CsI thin films for X-ray radiographic application. In: Mikhailin VV (ed) Proceeding of the fifth international conferences on inorganic scintillators and their applications, SCINT99. Moscow State University, Moscow, pp 391–397
60. Van Eijk CWE (2002) Inorganic scintillators in medical imaging. Phys Med Biol 47:R85–R106
61. Blasse G, Grabmaier BC (1994) Luminescent materails. Springer, Berlin, pp 84–162
62. Sonoda M, Takano M, Miyahara J, Kato H (1983) Computed radiography utilizing scanning laser stimulated luminescence. Radiology 148:833–838
63. Roques JP, Paul J, Mandrou P et al (1990) The sigma mission on the granat satellite. Adv Space Res 10:223–232
64. Patent PCT W001/60944
65. Patent PCT W001/60945
66. a Fernandez MM, Benlloch JM, Cerda J et al (2004) A flat-panel-based mini gamma camera for lymph nodes studies. Nucl Instr Meth Phys Res A527: 92–96. b Benlloch JM, Escat B, Fernández M et al (2003) Performance tests of a medical mini gamma-camera (summary). Nucl Instr Meth Phys Res A504: 232–233
67. Weisenberger AG, Bradley E, Majewski S, Saha M (1998) Development of a novel radiation imaging detector system for in vivo gene imaging in small animal studies. IEEE Trans Nucl Sci NS-145(3):1743–1749
68. Giokaris N, Loudos G, Maintas D et al (2004) Crystal and collimator optimization studies of a high-resolution γ-camera based on a position sensitive photomultiplier. Nucl Instr Meth Phys Res A527:134–139
69. Gektin AV, Gavryluk V, Boyarintsev AYu, Gayshan V (2003) Light spread function control for SPECT/PET systems. In: Second ITBS Conference, Milos, 26–30 May 2003 (abstracts), p 39
70. Bull U, Bartenstein P, Kirsch CM, Schicha H (2000) Combination systems for SPECT, coincidence, PET and CT. Technical spectrum, operating assumptions and possible areas of application. Nuklear Medizin 39(1):3–6
71. Delbeke D, Martin WH, Patton JA, Sandler MP (2001) Value of iterative reconstruction, attenuation correction, and image fusion in the interpretation of FDG PET images with an integrated dual-head coincidence camera and X-ray-based attenuation maps. Radiology 218(1):163–171
72. Patent France 2,237,206
73. Patton JA, Delbeke D, Sandler MP (2000) Image fusion using an integrated, dual-head coincidence camera with X-ray tube-based attenuation maps. J Nucl Med 41(8):1364–1368
74. McElroy DP, Huang S-C, Hoffman EJ (2002) The use of retro-reflective tape for improving spatial resolution of scintillation detectors. IEEE Trans Nucl Sci 49:165–171
75. Ricard M (2004) Imaging of gamma emitters using scintillation cameras. Nucl Instr Meth Phys Res A527:124–129
76. Trower WP, Korzhik MV, Fyodorov AA et al (1996) Cerium-doped lutetium-based single crystal scintillators. In: Dorenbos P, van Eijk CWE (eds) Inorganic scintillators and their application. Delft University Press, pp 355–358
77. http://www.researchandmarkets.com/research/ssgzrf/radiation
78. DNDO (2010) Letter from the Acting Director of DNDO to the Chairman of the Senate Committee on Homeland Security and Governmental Affairs, February 24, 2010

79. Burr1 T, Gavron A. Pass (2012) Fail criterion for a simple radiation portal monitor test. Mod Instrum 1:27–33
80. GAO-13-256 Report to Congressional Requesters (2013) Combating nuclear smuggling. Lessons Learned from Cancelled Radiation Portal Monitor Program Could Help Future Acquisitions
81. Wang X, Li J, Li Y, Cheng J et al (2007) Radiation portal monitor systems for SNM and other radionuclides. Detect Technol 27(620):634–637
82. Penn RD, Hood WE, Polichar RM, Cardone FH, Chavez LG, Grubbs SG, Huntley BP, Kuharski RA, Shyffer RT, Fabris L, Ziock KP, Labov SE, Nelson K (2011) A dual-sided coded-aperture radiation detection system. Nucl Instr Meth Phys Res A652:578–581
83. Technical Specifications of Mobile VACIS Inspection System (2007) http://www.saic.com/products/security/mobile-vacis/mobile-tech.html
84. Morris CL, Bacon J, Borozdin K et al (2014) Horizontal cosmic ray muon radiography for imaging nuclear threats. Nucl Instr Meth Phys Res B330:42–46
85. Goldberg M (1992) CApplications of scintillators in security inspection systems. In: Heavy scintillators for scientific and industrial applications, Proceedings of the "CRYSTAL 2000" International Workshop, Sept 22–26, 1992, Chamonix, France, pp 137–150
86. Ogorodnikov S, Petrunin V (2002) Processing of interlaced images in 4–10 MeV dual energy customs system for material recognition. Phys Rev Special Topics: Accelerators and Beams 5:104701
87. Grodzins L (1991) Nuclear techniques for finding chemical explosives in airport luggage. Nucl Instr Meth Phys Res B56/57:29–33
88. Naydenov SV, Ryzhikov VD (2003) Multienergy techniques for radiographic monitoring of chemical composition. Nucl Instr Meth Phys Res A505:556–558
89. Womble PC, Schultz FJ, Vourvopoulos G (1995) Non-destructive characterization using pulsed fast-thermal neutrons. Nucl Instr Meth Phys Res B99:757–760
90. SRPMs – ANSI N42.38 final publication IEC 62484. Performance Criteria for Spectroscopy-Based Portal Monitors used for Homeland Security
91. Vavilova IB, Bolotin YuL, Boyarsky AM, Danevich FA, Kobychev VV, Tretyak VI, Babyk IuV, Iakubovskyi DA, Hnatyk BI, Sergeev SG (2015) Dark energy and dark matter in the Universe: in three volumes. In: Shulga V (ed) Dark matter: observational manifestation and experimental searches, vol. 3. Akademperyodika, Kiev, Ucraine
92. Olive KA et al (Particle Data Group) (2014) Review of particle physics. Chin Phys C38: 090001
93. Bernabei R et al (2008) First results from DAMA/LIBRA and the combined results with DAMA/NaI. European Physical Journal C 56: 333. arXiv:0804.2741. J.Va'vra (2014) A new possible way to explain the DAMA results. Physics Lett B735: 181–185
94. Lee HS et al (KIMS Collaboration) (2014) Search for low-mass dark matter with CsI (Tl) crystal detectors Phys Rev D 90: 052006. arXiv:1404.3443
95. CRESST Collaboration (2014) Results on low mass WIMPs using an upgraded CRESST-II detector. http://arxiv.org/abs/1407.3146. European Physical Journal C 74: 3184
96. Kraus H et al (2006) EURECA – the European future of cryogenic dark matter searches. J Phys Conf Ser 39:139–141
97. Beeman JW, Bellini F, Benetti P (2005) Enriched ^{82}Se for the LUCIFER experiment. arXiv:1508.01709v1 [physics.ins-det] 7 Aug 2015
98. http://lz.lbl.gov/detector/
99. Band H, Cherwinka J, Heeger K, Hinrichs P, McFarlane M et al (2012) Low-background monitoring cameras for the Daya Bay antineutrino detectors. JINST 7: P08005, arXiv:1204.3500
100. Bernabei R et al (1997) Improved limits on WIMP – 19 F elastic scattering and first limit on the 2EC2_ 40Ca decay by using a low radioactive CaF2(Eu) scintillator. Astropart Phys 7:73–76

101. Belli P et al (2009) Search for double beta decay of zinc and tungsten with low background ZnWO4 crystal scintillators. Nucl Phys A826:256–273
102. Danevich FA et al (2003) Search for 2β decay of cadmium and tungsten isotopes: final results of the Solotvina experiment. Phys Rev C 68:035501
103. Cerulli R et al (2004) Performances of a BaF_2 detector and its application to the search for ββ decay modes in ^{130}Ba. Nucl Instr Meth Phys Res A525:535–543
104. Belli P et al (2003) Performances of a CeF_3 crystal scintillator and its application to the search for rare processes. Nucl Instr Meth Phys Res A498:352–361
105. Danevich FA et al (2001) Quest for double beta decay of ^{160}Gd and Ce isotopes. Nucl Phys A694:375–391
106. Arnaboldi C, Capelli S, Cremonesi O, Gironi L, Pavan M, Pessina G, Pirro S (2011) Characterization of ZnSe scintillating bolometers for Double Beta Decay. Astropart Phys 34:344–353
107. Danevich FA et al (2009) $MgWO_4$ – a new crystal scintillator. Nucl Instr Meth Phys Res A608:107–115
108. Cebrian S et al (2004) Bolometric WIMP search at Canfranc with different absorbers. Astropart Phys 21:23–34
109. Danevich FA et al (2011) Effect of recrystallisation on the radioactive contamination of $CaWO_4$ crystal scintillators. Nucl Instr Meth Phys Res A631:44–53
110. The ILIAS database on radiopurity of materials, http://radiopurity.in2p3.fr/
111. Zdesenko YG et al (2005) Scintillation properties and radioactive contamination of $CaWO_4$ crystal scintillators. Nucl Instr Meth Phys Res A538:657–667
112. Belli P et al (2011) Radioactive contamination of $ZnWO_4$ crystal scintillators. Nucl Instr Meth Phys Res A626–627:31–38
113. Belli P et al (2007) Investigation of decay of ^{113}Cd. Phys Rev C76:064603
114. Danevich FA et al (1996) Investigation of β + β + and β+/EC decay of ^{106}Cd. Z hysik A355:433–437
115. Georgadze AS et al (1996) Evaluation of activities of impurity radionuclides inцcadmium tungstate crystals. Instr Exp Technique 39:191–198
116. Danevich FA et al (2006) Application of $PbWO_4$ crystal scintillators in experiment to search for 2β decay of ^{116}Cd. Nucl Instr Meth Phys Res A556:259–265
117. Alessandrello A et al (1998) Measurements of internal radioactive contamination in samples of Roman lead to be used in experiments on rare events. Nucl Instr Meth Phys Res B142:163–172
118. Zdesenko YG et al (1996) Lead molybdate as a low-temperature scintillator in the experimental search for the neutrinoless double beta-decay of ^{100}Mo. Instr Exp Technique 39:364–368
119. Annenkov AN et al (2008) Development of $CaMoO_4$ crystal scintillators for a double beta decay experiment with ^{100}Mo. Nucl Instr Meth Phys Res A584:334–345
120. Barinova OP et al (2010) First test of Li_2MoO_4 crystal as a cryogenic scintillating bolometer. Nucl Instr Meth Phys Res A613:54–57
121. Barinova OP et al (2009) Intrinsic radiopurity of a Li_2MoO_4 crystal. Nucl Instr Meth Phys Res A607:573–575
122. Beeman JW et al (2012) A next-generation neutrinoless double beta decay experiment based on $ZnMoO_4$ scintillating bolometers. Phys Lett B710:318–323
123. Gironi L et al (2010) Performance of $ZnMoO_4$ crystal as cryogenic scintillating bolometer to search for double beta decay of molybdenum. JINST 5:11007
124. Danevich FA, Kobychev VV, Nagorny SS, Tretyak VI (2005) YAG:Nd crystals as possible detector to search for 2β and α decay of neodymium. Nucl Instr Meth Phys Res A541:583–589
125. Belli P et al (2007) Intrinsic radioactivity of a $Li_6Eu(BO_3)_3$ crystal and α decays of Eu. Nucl Instr Meth Phys Res A572:734–738

126. Balysh A et al (1993) Radioactive impurities in crystals of bismuth germanate. Pribory i Tekhnika Eksperimenta 1:118–122 (in Russian)
127. Coron N et al (2008) Our -short- experience at IAS and within ROSEBUD with radioactive contaminations in scintillating bolometers: uses & needs, presented at the Workshop on Radiopure scintillators for EURECA (RPSCINT 2008), 9–10 September 2008, Kyiv, Ukraine, p 12, arXiv:0903.1539
128. Wang SC, Wong HT, Fujiwara M (2002) Measurement of intrinsic radioactivity in a GSO crystal. Nucl Instr Meth Phys Res A479:498–510
129. Amare J et al (2006) Background understanding and improvement in NaI scintillators. J Phys Conf Series 39:201–201
130. Barton JC, Edgington JA (2000) Analysis of alpha-emitting isotopes in an inorganic scintillator. Nucl Instr Meth Phys Res A443:277–286
131. Bernabei R et al (2008) The DAMA/LIBRA apparatus. Nucl Instr Meth Phys Res A592:297–315
132. Lee HS et al (2007) Development of low background CsI(Tl) crystals for WIMP search. Nucl Instr Meth Phys Res A571:644–650
133. Zhu YF et al (2006) Measurement of the intrinsic radiopurity of ^{137}Cs/^{235}U/^{238}U/ ^{232}Th in CsI (Tl) crystal scintillators. Nucl Instr Meth Phys Res A557:490–500
134. Bernabei R et al (2005) Performances and potentialities of a $LaCl_3$:Ce scintillator. Nucl Instr Meth Phys Res A555:270–281
135. Belli P et al (2008) ^{7}Li solar axions: preliminary results and feasibility studies. Nucl Instr Meth Phys Res A806:388–397
136. Belli P et al (2007) Search for α decay of natural europium. Nucl Phys A 789:15–29
137. Ogawa I et al (2003) Double beta decay study of ^{48}Ca by CaF_2 scintillator. Nucl Phys A721:C525–C528
138. Argyriades J et al (2010) Results of the BiPo-1 prototype for radiopurity measurements for the SuperNEMO double beta decay source foils. Nucl Instr Meth Phys Res A622:120–128
139. Alimonti G et al (1998) Measurement of the ^{14}C abundance in a low background liquid scintillator. Phys Lett B422:349–358
140. Benziger J et al (2008) A scintillator purification system for the Borexino solar neutrino detector. Nucl Instr Meth Phys Res A587:277–291
141. Suekane F, Iwamoto T, Ogawa H, Tajima O, Watanabe H (for the KamLAND RCNS Group) (2004) An overview of the KamLAND 1-kiloton liquid scintillator. arXiv:physics/0404071
142. Dorr C, Klapdor-Kleingrothaus HV (2003) New Monte-Carlo simulation of the Heidelberg–Moscow double beta decay experiment. Nucl Instr Meth Phys Res A513:596–621
143. Klapdor-Kleingrothaus HV et al (2002) GENIUS-TF: a test facility for the GENIUS project. Nucl Instr Meth Phys Res A481:149–159
144. Kim KJ, Hasebe N (2012) Nuclear planetology: especially concerning the moon and mars. Research in Astron. Astrophys 12:1313–1380
145. Prettyman TH (2014) Remote chemical sensing using nuclear spectroscopy. In: Encyclopedia of the solar system. Elsevier, Amsterdam, pp 1161–1183
146. Yamashita N, Gasnault O, Forni O, d'Uston C, Reedy RC, Karouji Y, Kobayashi S et al (2012) The global distribution of calcium on the moon: implications for high-Ca pyroxene in the eastern mare region. Earth Planet Sci Lett 353–354:93–98
147. Hansson CCT, Owens A, Shortt B, Dorenbos P, Quarati F, Williams R, Hahn D, Toepfer T, Pathier L, Schotanus P, v.d. Biezen J, O'Neill KN, Jackson C (2012) Development of low noise scintillator crystals for planetary space missions. In: L. Wall, 2012 Nuclear science symposium and medical imaging conference record (NSS/MIC), ISMA, Kharkov, Ukraine, N14-241, pp 927–930
148. Kozyrev A, Vostrukhin A, Litvak A et al (2009) Application of scintillation detectors in space investigation of sun system bodies and astrophysical objects. In: Scintillation materials. Engineering, devises, applications. ISMA, Ukraine, pp 23–55

149. Zhu M, Chang J, Ma T, Ip WH, Fa W, Wu J, Cai M et al (2013) Potassium m ap from Chang'E-2 constraints the impact of Crisium and Orientale basin on the moon. Sci Rep 3:1611
150. Kraft S, Maddox E, Buis E-J, Owens A, Quarati FGA, Dorenbos P, Drozdowski W, Bos AJJ, de Haas JTM, Brouwer H, Dathy C, Ouspenski V, Brandenburg S, Ostendorf R (2007) Development and characterization of large La-halide gamma ray scintillators for future planetary missions. IEEE Trans Nucl Sci 54:873–878
151. Owens A, Bos AJJ, Brandenburg S, Buis E-J, Dathy C, Dorenbos P, van Eijk CWE, Kraft S, Ostendorf RW, Ouspenski V, Quarati F (2007) Assessment of the radiation tolerance of LaBr3:Ce scintillators to solar proton events. Nucl Instr Meth Phys Res A572:785–793
152. Drozdowski W, Dorenbos P, Bos AJJ, Bizarri G, Owens A, Quarati FGA (2008) CeBr3 scintillator development for possible use in space missions. IEEE Trans Nucl Sci 55(3):1391–1396
153. Dean AJ (1992) Imaging is high energy astronomy. In: DeNotaristefani F, Lecoq P, Schneegans M (eds) Heavy scintillators for scientific and industrial applications. Frontieres, Gif-sur-Yvette, pp 53–64
154. BaBar Collaboration (1995) BaBar technical design report, SLAC-R-95-457
155. INTEGRAL Assessment Study Report (1991) ESA Publication ESA SCI 91, pp 1–31
156. Ubertini P, Cocco GD, Lebrun F (1997) The IBIS telescope on board INTEGRAL. In: Proceeding of the Second INTEGRAL Workshop, ESA SP-382, p 599. a Barbiellini G, Boezio M, Casolino M et al (1991) The GILDA mission: a new techniques for γ-ray telescope in the energy range 20 MeV – 100 GeV. http://ifctr.mi.cnr.it/agile. b Mergeletti S, Barbiellini G, Budini et al (1999) GeV-TeV γ-ray Astrophysics. Workshop "Towards a Major Atmospheric Cerenkov Detector VI". Snowbird, Utah, 11–23
157. http://cossc.gsfc.nasa.gov/
158. Johnson WN, Grove JE, Phlips BF et al (2001) The construction and performance of the CsI hodoscopic calorimeter for the GLAST beam test engineering module. IEEE Trans Nucl Sci 48:1182–1189
159. Atwood WB, Ritz S, Anthony P et al (2000) Beam test of γ-ray large area space telescope components. Nucl Instr Meth Phys Res A446:444–460
160. Shwarz B (2000) Electromagnetic calorimeter of the BELLE detector. In: Mikhailin VV (ed) Proceeding of the fifth international conferences on inorganic scintillators and their applications, SCINT99. Moscow State University, Moscow, pp 186–190
161. Gektin AV, Gavrylyk V, Zosim D (2000) Long Length Scintillators for the Position Sensitive Radiation Detectors, IEEE NSS/MIC. Abstracts, p 263
162. Gektin AV, Zosim D, Boyarintsev AY et al (2004) Long position sensitive CsI(Tl) detectors for the GLAST project. In: IEEE Nuclear Science Symposium and Medical Imaging Conference, Abstracts, N16-7, p 45
163. Fertl WH, Chilingar GV (1988) Total organic carbon content determined from well log. SPE Form Eval 3(2):407–419
164. Saint Gobain Crystals Catalogue
165. Glodo J, van Loef E, Hawrami R, Higgins WM, Churilov A, Shirwadkar U, Shah KS (2011) Selected properties of Cs2LiYCl6, Cs2LiLaCl6, and Cs2LiLaYBr6 scintillators. IEEE Trans Nucl Sci 58:333–338
166. Van Loef EVD, Glodo J, Higgins WM, Shah KS (2005) Optical and scintillation properties of Cs2LiYCl6: Ce3+ and Cs2LiYCl6: Pr3+ crystals. IEEE Trans Nucl Sci 52:1819–1822
167. Dorenbos P (2000) The 5d level positions of lhe trivalent lanthanides in inorganic compounds. J Luminescence 91:155
168. Dorenbos P (2000) 5-d levels energies of Ce3+ and the crystalline environment. I. Fluoride compounds. Phys Rev B 62:15640
169. Barishevsky VG, Zouevski RF, Korlhik MV et al (1991) Fast scintillators $YAIO_3$:Pr. Pis'ma v JTP 17:82

170. Nikl M, Ogino H, Krasnikov A, Bietlerova A, Yoshikawa A, Fukuda T (2005) Photo-and radioluminescence of Pr doped $Lu_3Al_5O_{12}$ single crystal. Phys Stat Sol (a) 202:R4
171. Borisevitch A, Korjik M, Mechinsky YV (2010) On the development of scintillation materials operating at high temperature. Nuclear Science Symposium Conference Record (NSS/MIC), IEEE: 571–573
172. US patent 7019284B2, Mar., 28, 2006
173. Ablard P, Bell C, Cook D et al (2012) The expanding role of mud logging. Oilfield Rev 24(1):24–41

http://www.springer.com/978-3-319-45521-1

Inorganic Scintillators for Detector Systems
Physical Principles and Crystal Engineering
Lecoq, P.; Gektin, A.; Korzhik, M.
2017, XVI, 408 p. 226 illus., 44 illus. in color., Hardcover
ISBN: 978-3-319-45521-1